Technische Universität München
Fakultät für Physik

Gamma-Ray Flashes from Classical Novae
Gamma Flashes von klassischen Novae

Juan Agustin Urruty

First Supervisor: Dr. Jochen Greiner

A thesis presented for the degree of
Bachelor of Science

Max Planck Institute for Extraterrestrial Physics

Munich, the 20th of September 2022

Abstract

The last several years and decades have seen the rise of multi-wavelength astronomy, and only by continuing with this endeavour can we hope to understand the physical processes in the universe. Despite years of gamma-ray studies coming from classical novae, no experiment ever claimed to have measured these. My goal is to use theorised models and time-resolved spectra in combination with INTEGRAL/SPI to try and measure them. I generated a catalogue with reasonable candidates, and upon analysing them, I found high significance coming from 4 novae hinting at gamma-ray flashes. These results were consequently compared with INTEGRAL/IBIS, which rather than prove them, it challenged them. Thus I conclude that there is some evidence of gamma rays leaving the nova while it is transparent.

Dedication

To mum and dad, who helped me go through this long journey of studying abroad and always provided me with what was necessary. I will always appreciate all they have done.
To my homeland Uruguay, and some teachers from my school in Paysandu, who gave me the motivation to pursue this dream of graduating in Physics in Germany.

Declaration

I declare that this thesis is an original report of my research, has been written by me and has not been submitted for any previous degree. The experimental work is almost entirely my own work; the collaborative contributions have been indicated clearly and acknowledged.

Juan Agustin Urruty

20.09.22

Date

Acknowledgements

I would like to express my gratitude to Dr. Thomas Siegert, who guided me throughout this project. I would also like to show my deep appreciation to my primary supervisor, Dr. Jochen Greiner, who took care of a lot of the logistics and also organised a weekly seminar to pass on his knowledge and help us develop our presentation skills. As for the funding organisations, this work would not have been possible without the support of the Max Planck Institute for Extraterrestrial Physics and the Technical University of Munich.

Contents

CHAPTER 1

Introduction

Gamma-ray (GR) flashes are highly energetic electromagnetic events happening throughout the universe, and we on the Earth can measure them from billions of light years away. Knowing the processes taking place out there we can expect GR signatures from several source types. For instance, from nucleosynthesis in classical novae (CNe) we would expect to detect GR lines - in fact, novae are considered potential GR emitters since 1974 as suggested by Clayton and Hoyle (1974, [4]).
Since then, a great deal of methods to measure GR have been proposed, and many satellites that are sensitive to GR like INTEGRAL/SPI, Fermi/GBM, and Swift/BAT have been successfully commissioned [29].
Most of these satellites were launched in the early 2000s, and are still active as of today (2022) orbiting our earth and looking at our sky. From Shafter's work [20] we expect a novae occurrence rate in the Milky Way of (50 ± 25) yr^{-1}, from these 50 only 20% are seen in ultraviolet, optical, and infrared wavelengths. As we go up in energy, at GeV, we only have a handful of analysed objects during the whole mission of our detectors. Most GR flashes lie at the MeV energy range, and they have never been observed coming from CNe - neither individually at the time of the explosion, as a result of radioactive decay, nor the diffuse galactic emission from the novae population. A recent study from Leung and Siegert (2022, [14]) shed some light on possible reasons why; they simulated several CNe and analysed the fluxes from characteristic lines like the 511 keV one and found that the flash at the time of the explosion was at least a million times fainter than earlier predicted [12]. This means that CNe need to be no further away than a few hundred parsec for our satellites to detect them, yet most of them are at a distance of around 10 kpc [24].
In this work I will first generate a novae catalogue with reasonable candidates, then take time-resolved spectra from [24] and fit them to measures taken from INTEGRAL/SPI. These measures must have happened in a time window of 14 days before the detection of the nova; as we shall see later, when a nova is detected, the GR-flash has already happened.
Measuring GR flashes coming from CNe could give us insight into the explosion mechanism as well as nucleosynthesis products. It could also check if the prediction of novae per mission lifetime is useful with a retrospective analysis.

CHAPTER 2

Theory

2.1 Gamma-ray emission

2.1.1 Production

Gamma radiation lies at the high end of the electromagnetic spectrum, and thus only processes with such energy can produce it.
In this section, I will explain the two main GR production mechanisms.

Radioactive decay

This is the most common type of production; in atomic nuclei, we can find protons (p^+) and neutrons (n°), stabilised by the strong nuclear force between nucleons against, and the Coulomb potential between protons and electrons (e^-). However, for some atoms the quantity of these particles drifts away from the equilibrium state, and it is no longer stable. Consequently, it will spontaneously emit particles to get back to a stable state. In some cases, here is where the process stops, but in the majority, the daughter nucleus is not necessary stable and keeps emitting particles until it reaches stability. In such case we speak about a decay chain, with one

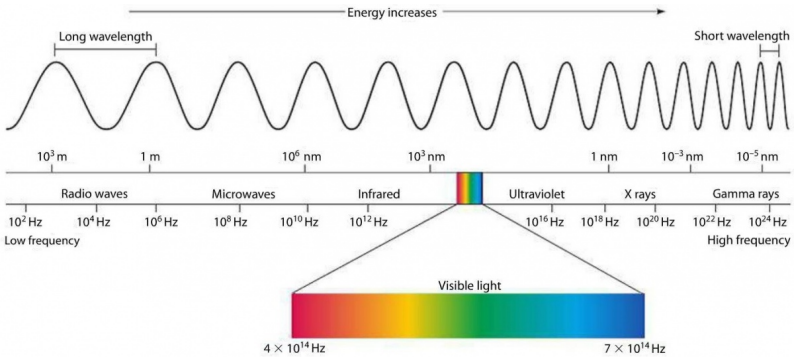

Figure 2.1: Electromagnetic spectrum, gamma rays have the highest energy and shortest wavelength. Source: *Imperial Encyclopedia* [25]

initial (unstable) state, one final (stable) state, and potentially many in between. Depending on the type of particle that the nucleus emits, we can classify these decays.
If a particle consisting of two p^+ and two n° (a ^{4}He nucleus) gets emitted, we call it α-decay, this is a process of the strong nuclear force and can be described with the equation:

$$ {}^{\mathrm{A}}_{\mathrm{Z}}\mathrm{X} \longrightarrow {}^{\mathrm{A}-4}_{\mathrm{Z}-2}\mathrm{Y} + {}^{4}_{2}\alpha \tag{2.1} $$

with X being the parent nucleus, Y being the daughter nucleus, and A and Z being the mass and atomic number, respectively.

Now we get into the decay which lead to the discovery of the weak nuclear force: the β-decay. Here we must distinguish between three subtypes; the β^+ and β^--decay, which only differ in the emitted particles being matter of antimatter[1], and finally the electron capture (also called inverse β-decay), where particles are not only emitted but also absorbed.
The β^+-decay is, as well as the remaining two, a process of the weak nuclear force where a p^+ inside the atomic nucleus decays into a positron (e^+) and a n°, together with an electron-neutrino (ν_e) to keep the energy and lepton number conserved. The equation of the reaction reads:

$$ {}^{\mathrm{A}}_{\mathrm{Z}}\mathrm{X} \longrightarrow {}_{\mathrm{Z}-1}{}^{\mathrm{A}}\mathrm{Y} + e^+ + \nu_e \tag{2.2} $$

This process happens to nuclei with too many protons, such as ^{13}N, or ^{22}Na. Similarly, if there are too many neutrons, β^--decay will be favoured. Here, a neutron decays into a proton and an electron under emission of an electron-anti-neutrino ($\overline{\nu_e}$). The reaction is:

$$ {}^{\mathrm{A}}_{\mathrm{Z}}\mathrm{X} \longrightarrow {}_{\mathrm{Z}+1}{}^{\mathrm{A}}\mathrm{Y} + e^- + \overline{\nu_e} \tag{2.3} $$

As for the electron capture, a shell electron (usually from the innermost K-shell) is captured in the nucleus. This happens to atoms with large nuclear radius and small shell radius, where the wave functions can overlap. The shell electron and a proton in the nucleus unite to form a neutron, and the effect on the nucleus is the same as in the β^--decay:

$$ {}^{\mathrm{A}}_{\mathrm{Z}}\mathrm{X} + e^- \longrightarrow {}_{\mathrm{Z}-1}{}^{\mathrm{A}}\mathrm{Y} + \nu_e \tag{2.4} $$

In β-decay there are always three elements taking part, which is why the spectrum has continuous appearance.
In general, after either α or β-decay the atom is often left in an excited state, and by gamma emission it can de-excite into its ground-state. This last process is called γ-decay, and represented with following equation:

$$ ({}^{\mathrm{A}}_{\mathrm{Z}}\mathrm{X})^* \longrightarrow {}^{\mathrm{A}}_{\mathrm{Z}}\mathrm{X} + \gamma \tag{2.5} $$

In Fig. 2.2 are some examples graphically shown.

[1]The standard model of particle physics states that to every particle there is an anti-particle, which has the same Spin and mass as the first particle, but opposite charge.

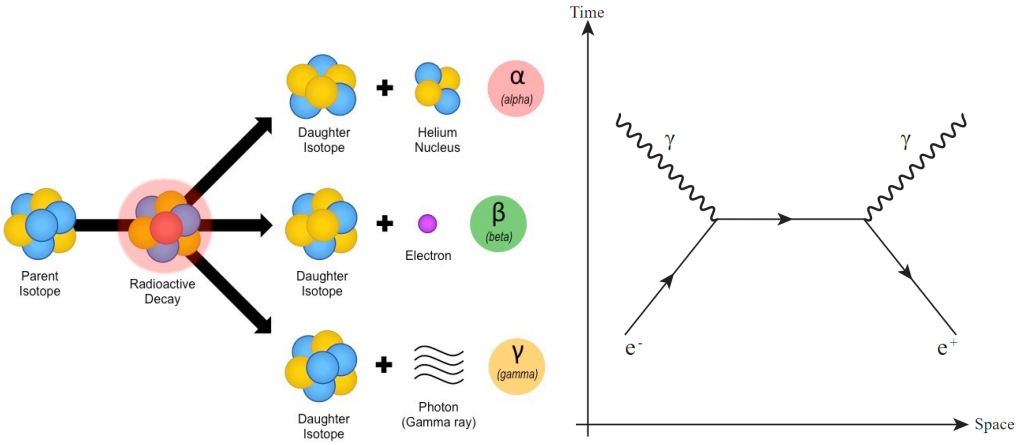

Figure 2.2: Left: Diagram of the three most common radioactive decays. Right: Feynmann Diagram of electron-positron annihilation.

Electron-Positron annihilation

According to the standard model each particle has its own anti-particle, and when they interact, at low they annihilate leaving only energy in form of gamma emission as a product, according to Einstein's equation: $E^2 = (mc^2)^2 + (pc)^2$, with m being the rest mass of the particle and p its momentum. At high energies, other particles, such as B mesons or the W and Z bosons, can be created. If an electron annihilates with a positron (both at rest), two photons will result, each carrying the energy of 511 keV.
Another possibility is that they form a bound quantum state called *Positronium*, this can exist in one of two states; if the spins of e^- and e^+ are anti-parallel, the state is called para-positronium. If they are aligned parallel, we speak of ortho-positronium. Para-positronium has an average lifetime of 125 ns, and will subsequently decay into two photons, while ortho-positronium has an average lifetime of 142 ns, before it decays into three photons. These photons will carry at most 511 keV, which is why the spectrum has a clear line at that energy and a tail behind it.

2.1.2 Interactions with matter

To complete the GR theory section, I will explain the ways they interact with matter, mostly because the only way for us to measure them, is by interacting with them. I will mention the three most important mechanisms, and give a brief overview from each of them.

Photoelectric absorption

This interaction, which earned Albert Einstein his Nobel Prize, is dominant at low energies (below 50 keV), and it happens when a gamma photon interacts with an atomic electron, passing it all its energy, causing the ejection of the electron from the atom. The kinetic energy of this so-called *photoelectron* is given by:

$$E_{kin,e^-} = h\nu - E_b \tag{2.6}$$

where ν is the frequency of the absorbed photon, h the Planck's constant, and E_b the binding energy of the photoelectron to the atom. The atom is left ionised, and

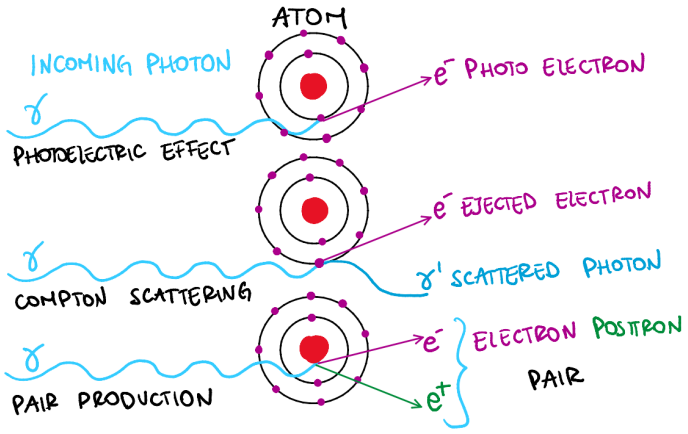

Figure 2.3: Schematic view of the three main processes accounting for GR interaction and absorption. Physical accuracy was compromised to make the effect clear. In reality, the nucleus is about 1 fm wide and the whole atom 100000 times bigger, secondly, electrons do not orbit in defined paths but obey Heisenberg's uncertainty principle. The places where is more probable to find them go according to the spherical harmonics.

will either catch an electron from the neighbourhood or rearrange its electrons to fill the vacancy. This leads to a new photon being emitted.

Compton scattering

In this case, an incoming gamma photon loses enough energy to an (atomic or free) electron to cause its ejection, and the remainder of the photon's energy is re-emitted as a new, lower-frequency photon. Also, the direction of the emitted photon is changed, hence the term "scattering". This is the principal absorption mechanism at energies of 100-10000 keV. The wavelength difference of the photons is given by:

$$\lambda' - \lambda = \frac{h}{m_e c}(1 - \cos\theta) \tag{2.7}$$

with $m_e c$ the energy of the electron, and θ the scattering angle.
This effect is very important for us, as it is possible for the gamma rays to scatter out of the detectors, thus influencing the measure.

Pair production

At high energies, exceeding 1022 keV, pair production becomes possible, and at around 10 MeV it becomes the most important. When entering the electric field of a nucleus, the energy of the gamma photon becomes an electron-positron pair, hence the minimum necessary energy 1022 keV = 2 times the resting mass of the electron or positron, 511 keV. At higher photon energies, the remaining goes into kinetic energy to conserve momentum. The created positron will rapidly annihilate with an electron, leading to two GRs with energies of at least 511 keV.

We can define the total absorption/attenuation which a material imparts to a photon as:

$$I(x) = I_0 \cdot \exp(-\mu x) \tag{2.8}$$

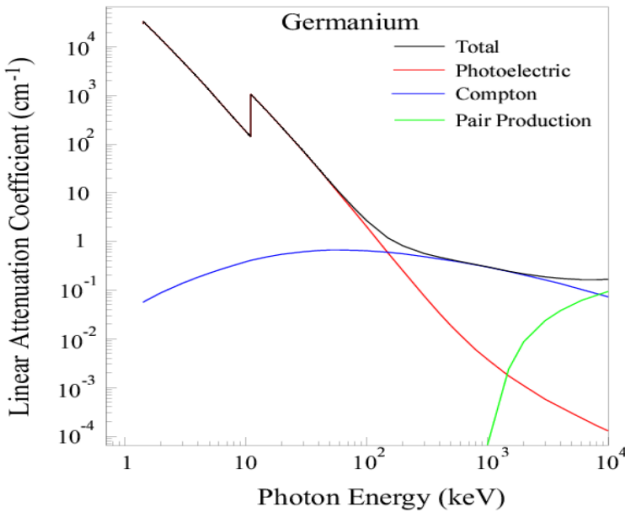

Figure 2.4: The total absorption coefficient of germanium (atomic number 69) for gamma rays, plotted versus gamma-ray energy, and the contributions by the three effects. For most materials, the photoelectric effect is largest at low energies, Compton scattering dominates at intermediate energies, and pair production dominates at high energies. The abrupt steps in the photoelectric effect is due to the electron shells of the atom.

where I_0 is the initial intensity of the photon, and μ the absorption coefficient. This varies from material to material, and it will represent how much of a given intensity of a photon with a given frequency a material can absorb (and thus measure). In Fig. 2.4 we can see the total absorption coefficient of Germanium, the material present in our GR detector SPI (see Section 3.2).

2.2 Classical Novae

The reason I made this thorough explanation of GR is that these processes both occur in Classical Novae (CNe) and are used to measure high-energy photons.

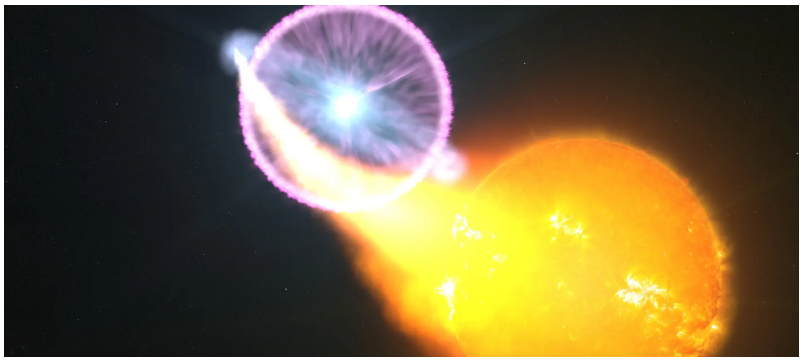

Figure 2.5: Impression of a nova. In front we can see a main sequence star, and behind a white dwarf accreting matter from it. This phase is called "Quiescence", where the outburst hasn't yet taken place. Source: *Nasa's goddard space center*

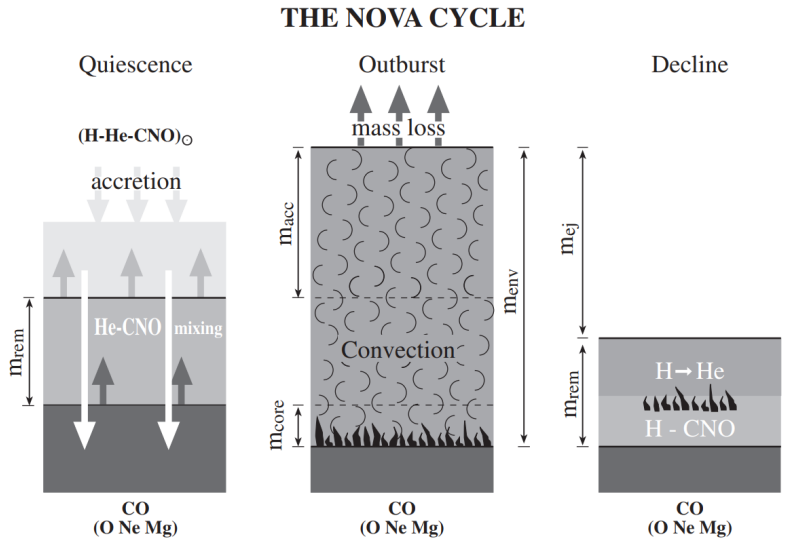

Figure 2.6: The nova cycle with the three phases, the quiescence before the outburst, and lastly the decline, after the fuel is exhausted. The white dwarf's mass mixed into the nova envelope is denoted m_{core}; the remnant envelope mass after completion of mass ejection is denoted m_{rem}. m_{acc} is the accreted mass, and m_{ej} the ejected mass. This diagram focuses on composition changes caused by mixing, convection, and nuclear burning. CO and O Ne Mg stand for the two main types a WD can be composed of, depending on its mass. [15]

A Nova is a transient[2] astronomical event which causes the appearance of a very bright, "new" star. This is the reason why they were firstly referred to as *"nova stella"* (Latin for new star), hence the name we use today.
This apparent "new" star brightens several hundred- to a million-fold, remains bright for a few days to several months and then returns to its former, low luminosity[11]. As we shall see later, the spectrum also changes a lot during this period. Although it is thought that all novae are recurrent, some of them take hundreds to thousands of years to brighten again. These are referred to as CNe to distinguish them from faster[3] recurrent novae. After years of observations and theories, we now have a detailed model of CNe, which will be explained next.

CNe are created in a close binary star system consisting of a white dwarf (WD) and either a main sequence, subgiant, or red giant star. The WD, being much more massive than its companion, will start to accrete[4] matter (mostly hydrogen) from it onto its surface, creating a dense but shallow atmosphere. WDs are already very dense objects, being the remnant of a stellar core, the extreme conditions makes gravity want to collapse all matter into a single point. The reason why it does not happen lies in the nature of the WD's composition; electron-degenerate-matter. Electrons, forming part of the fermion family obey the Pauli exclusion principle[5]

[2]To contrast it to the timescale of the millions or billions of years during which the galaxies and their component stars in our universe have evolved

[3]Recurrent periods of 10-100 years

[4]Means "draw to itself", or more familiar "suck"

[5]States that two or more identical particles with half-integer spins (i.e. fermions) cannot occupy the same quantum state within a quantum system simultaneously.

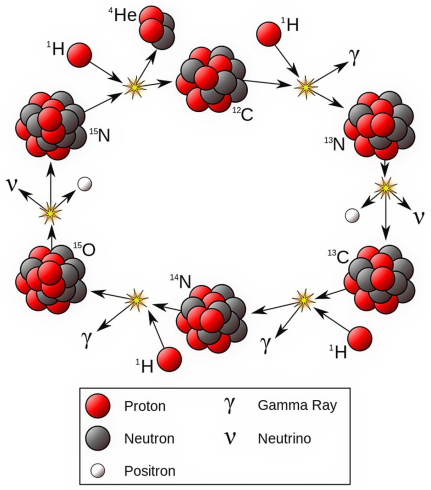

Figure 2.7: The CNO-cycle. It starts with a ^{12}C capturing a proton producing ^{13}N which will subsequently undergo β^+-decay, emitting a photon and leaving a ^{13}C which yet again captures another proton, turning into ^{14}N and emitting another photon. After capturing another proton, ^{14}N becomes ^{15}O which undergoes another β^+-decay, leaving behind a ^{15}N. This will capture a photon and undergo α-decay, leaving the ^{12}C we started with. Source: *ESO Supernova* [3]

and thus cannot collapse into a single point. This pressure at very high densities of about $1 \times 10^9\,\mathrm{kg\,m^{-3}}$ and relativistic electron energies from 2.5 keV upwards is given by:

$$P = K \cdot \rho^{4/3} \tag{2.9}$$

where K is a proportionality constant depending on the properties of the particles making up the gas. Note that this pressure is independent of the temperature.
As more hydrogen-rich matter is accreted, the temperature at the WD's surface begins to rise due to friction. At this point, an ideal gas would expand to cool down, but as WDs are not, and the pressure does not depend on T, expansion is not a possibility and T will rise higher. [24] This leads to a vicious circle where the temperature rises without bound, and at around 20 MK, hydrogen burning will set in and the CNO-cycle begins (see Fig. 2.7). This whole process is called thermonuclear runaway, and after several iterations, the radiation pressure of the burning surface will lead to the ejection of matter. [15]

Most of this matter can be seen in visible light using telescopes like Hubble or the new JWSP (or even amateur telescopes on earth) and is what was earlier mistaken as a "new" star. However, a number of radioactive elements will also get ejected and decay according to section 2.1.1. There are two main CNe types, CO CNe having a WD composed by carbon and oxygen and ONe CNe, with a WD formed mainly by oxygen, neon and magnesium. If the mass of the progenitor is around $8-10.5M_\odot$, then the core temperature will be sufficient to fuse carbon but not neon leading to a ONe CNe. Progenitor masses of $0.5-8M_\odot$ will only lead to CO CNe. The 4 main isotopes which are synthesised in the CNe are ^{13}N, with a production of around $10^{-9}-10^{-6}M_\odot$, ^{18}F with a production between $10^{-8}-10^{-5}M_\odot$, and ^{7}Be with a range between $10^{-12}-10^{-11}M_\odot$. These three elements do not vary much

between the WD's composition. However, ^{22}Na production is 10-100 times higher in ONe WDs than CO, these last having a production range of between $10^{-12} - 10^{-10} M_\odot$ [14]. The synthesis mechanism of these elements is believed to occur via $^3\mathrm{He}(\alpha,\gamma)^7\mathrm{Be}$ for beryllium, via proton captures together with $\gamma-$ and β^+-decay for ^{22}Na ($^{20}\mathrm{Ne}(p,\gamma)^{21}\mathrm{Na}(p,\gamma)^{22}\mathrm{Mg}(\beta^+)^{22}\mathrm{Na}$ or $^{20}\mathrm{Ne}(p,\gamma)^{21}\mathrm{Na}(\beta^+)^{21}\mathrm{Ne}(p,\gamma)^{22}\mathrm{Na}$) [24]. As for fluorine, the syntesis mechanism is given by $^{14}\mathrm{N}(\alpha,\gamma)^{18}\mathrm{F}$. Elements whose production was not cited here, are a by-product of the CNO-cycle. The reactions of these most abundant radioactive elements in a CNe are:

$$^{13}_{7}\mathrm{N} \longrightarrow {}^{13}_{6}\mathrm{C} + e^+ + \nu_e + 1950\,\mathrm{keV} \qquad (\tau \approx 14\,\mathrm{min}) \tag{2.10}$$

$$^{18}_{9}\mathrm{F} \longrightarrow {}^{18}_{8}\mathrm{O} + e^+ + \nu_e + 630\,\mathrm{keV} \qquad (\tau \approx 160\,\mathrm{min}) \tag{2.11}$$

$$^{22}_{11}\mathrm{Na} \longrightarrow {}^{22}_{10}\mathrm{Ne} + e^+ + \nu_e + 1275\,\mathrm{keV} \qquad (\tau \approx 2.6\,\mathrm{yr}) \tag{2.12}$$

$$^{7}_{4}\mathrm{Be} + e^- \longrightarrow {}^{7}_{3}\mathrm{Li} + \nu_e + 478\,\mathrm{keV} \qquad (\tau \approx 77\,\mathrm{days}) \tag{2.13}$$

The γ-decay is also appended to the equation. Also, τ represents the half-life of each atom. This will be important for our models later, as it gives information about when these reactions will take place and for how long.

As mentioned in the introduction, no one has ever managed to measure these GRs, which we know are there from well-studied WDs and main sequence stars, leaving a large gap in the understanding of nucleosynthesis in these events.

2.2.1 CNe simulation

It is believed that the ejected material of a CN is about $10^{-4} M_\odot$ and the speeds of hundreds to thousands of km per second. The flux is estimated to be around $0.001\,\mathrm{ph\,cm^{-2}\,s^{-1}}$.

In late 2021, Leung and Siegert [14] developed numerical models of nova explosions using CO white dwarfs as the progenitor. They arrived at several times smaller ejecta velocities, and fluxes of $1 \times 10^{-9}\,\mathrm{ph\,cm^{-2}\,s^{-1}}$ for distances of 1 kpc, disagreeing with today's expectations. This hinted why, having novae such a high occurrence rate in the Milky Way, were never detected in GR.

With their model they were also able to gauge the distance such a nova would have to be for our current most sensitive telescope SPI to detect it, being at most 100 pc. As seen in Fig. 2.8, most CNe are not at such distances, rendering my chances of measuring these GR quite insignificant.

However, the simulations also produced time-resolved spectra showed in Fig. 4.5, which will enhance the sensitivity of our detector.

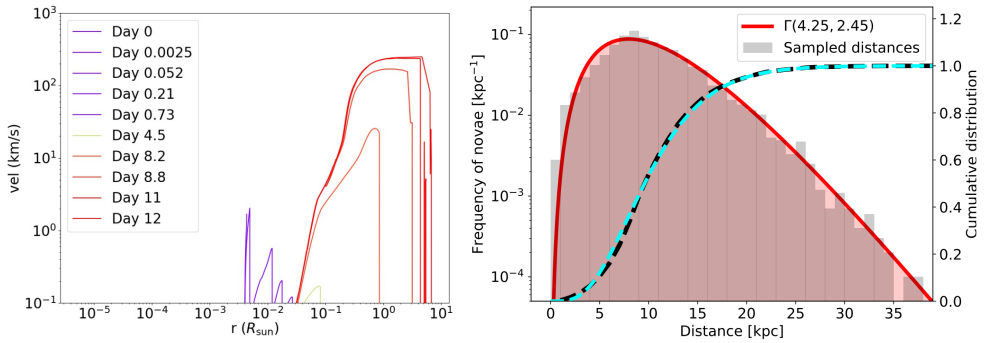

Figure 2.8: Left: Plot of the velocity profiles for a CNe of 1.3 solar masses. Related to the radius of the WD and at different times. At the beginning most of the mass is close to the star, and moving relatively slow. As time passes, we find matter further away from the star, and moving at much higher speeds. Right: Distance distribution of CNe corresponding to a time window of 200 yr. The cumulative distributions are shown in black for the sample and in cyan for the Γ-distribution (right axis)[14] [24]

CHAPTER 3

Instruments

In this thesis, I will work mainly with the satellite INTEGRAL and its instrument onboard, SPI. I will therefore give a compact explanation of what they are and how they operate.

3.1 The INTEGRAL mission

The ESA observatory INTEGRAL (International Gamma-Ray Astrophysics Laboratory) is dedicated to the fine spectroscopy and fine imaging of celestial GR sources in the energy range 15 keV to 10 MeV, in the MeV range its the most sensitive observatory in space we have to date [26]. It was launched on 17 October 2002 and it is still active as of the writing of this thesis. It was inserted into a 72-hour long highly eccentric orbit (perigee at 9000 km and apogee at 154000 km) [29]. The motive for this orbit is to provide long periods of uninterrupted observation with a nearly constant background and away from trapped radiation (electron and proton Van Allen belts). The triggering thresholds for the instruments shutdown are 40000 km when approaching the earth and 60000 km when leaving the earth, which ensures a utilisable orbit of about 90%. Each of these orbits are called "revolutions". Furthermore, there is a particle radiation monitor on-board which gives us information about the radiation in the local environment of the spacecraft. The INTEGRAL payload consists of 4 instruments: two dedicated for GR being the spectrometer SPI and the imager IBIS, as well as two monitors being JEM-X for x-rays and OMC for the optical spectrum. SPI and IBIS are made in such a way that the weaknesses of one are the strengths of the other, complementing each other. For instance, SPI has a high spectral resolution of 3 keV at 1.7 MeV and an angular resolution of around 2.5 degrees. IBIS, in contrast, has a spectral resolution of 8 keV at 100 keV, making it 45 times less[1] detailed than SPI, but has an angular resolution of 12 arcmin, being about 13 times more detailed than SPI. The energy range at which they operate is about the same; 18 keV to 8 MeV for SPI and 15 keV to 10 MeV for IBIS. IBIS's

[1]This is not as meaningful as the angular resolution, because it is subject to the energy it is currently measuring. In fact, SPI is more sensitive than IBIS from 500 keV onwards.

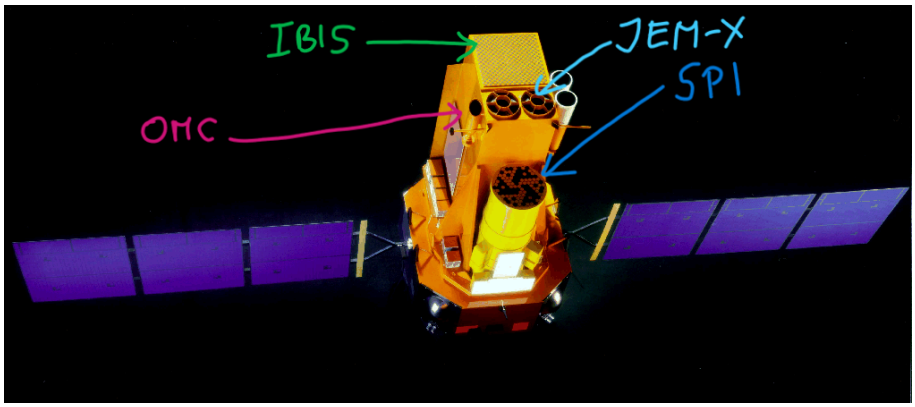

Figure 3.1: The INTEGRAL spacecraft. In a cylindrical shape, covered by the tungsten mask hides the SPI instrument. The other instruments can also be seen *Source: ESA* [1]

timing accuracy is about 2 times more fine than that of SPI, having 61 µs and 126 µs respectively. [29]

3.2 The SPI instrument

The most important instrument aboard the satellite for us is the Spectrometer on INTEGRAL (SPI), which I will use throughout this whole thesis. This telescope can measure the energy coming from GR with very high spectral resolution in the range of 18 to 8000 keV divided into 3 sections; SE (18-600 keV), PSD (514-2000 keV) and HE (2000-8000 keV). It has a field of view of 16 by 16 degrees, and an angular resolution of 2.5 degrees at FWHM [29]. It consists of a honeycomb-shaped array of 19 germanium detectors surrounded by an active anticoincidence shield (ACS), and a coded mask made of tungsten seen in figure 3.4 [27].
I will first explain the coded mask; it is situated 1.71 m above the detector and is half covered by tungsten plates in a pattern with 120-degree rotational symmetry. The reason for this is so that SPI knows from which part of the sky is the photons are coming. Having this symmetry and arrangement, the intensity measured by the germanium detectors gets coded by the direction of entrance in the instrument (seen in Figure 3.3). The ACS is made from Bismuth Germanate (BGO) scintillator crystals and photomultiplier tubes, which together with the Plastic Scintillator Anti Coincidence Subassembly (PSAC) can filter events originating from prompt cosmic-ray interactions. When triggered, registration of SPI events by the Germanium detectors is disabled for 725 ns.[6] [18]

The high-purity germanium crystals fall into the category of semiconductors. The reason we want semiconductors to be the GR detectors is because of their physical properties; there is an energy gap between the valence band and the conduction band[2], and it is small enough for electrons to jump and create electron-hole-pairs.

[2]The valence band is lower in energy, filled with electrons located in the outer atomic shells taking part in the covalent bonding within the crystal. The conduction band is higher in energy usually containing no electrons, however, if the energy required to bridge the gap is reached, an electron can jump creating a hole in the valence band and move freely in the conduction band,

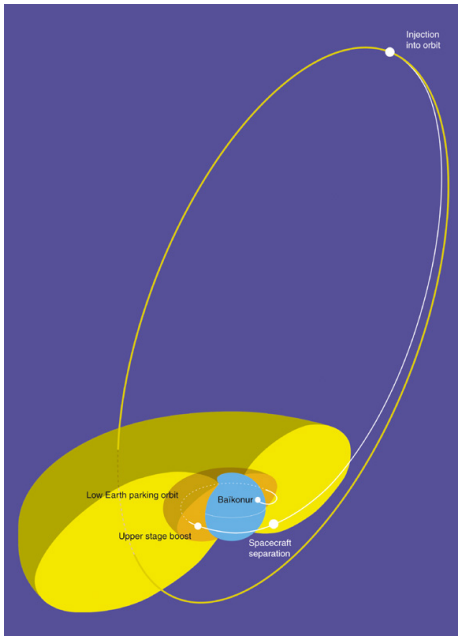

Figure 3.2: The eccentric orbit of INTEGRAL. Shown in yellow and orange are the radiation belts, where the instruments aboard INTEGRAL shut down until the spacecraft is back outside. *Source: ISDC*

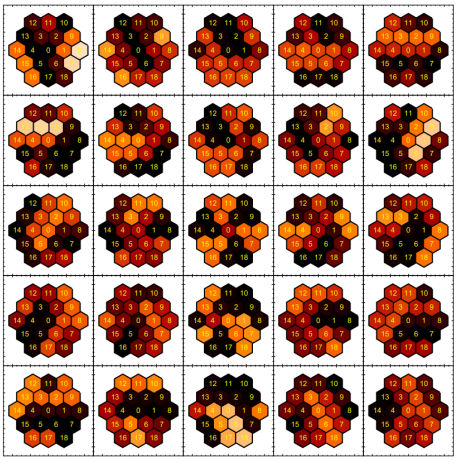

Figure 3.3: The shawdowgrams seen in the detector cast from the coded mask. Detectors are numbered inside-out, starting from 0 for the central detector. Intensity received by each detector is colour-coded from black (none;shadowed) through red, yellow to white (full exposure). The 25 panels are due to the systematic orientation variance INTEGRAL does around the direction of the target in steps of 2.1 degrees called "dithering" and it produces additional modulation of the imaging information. This usually results in a 5 by 5 grid *Source: Diehl et al.[6]*

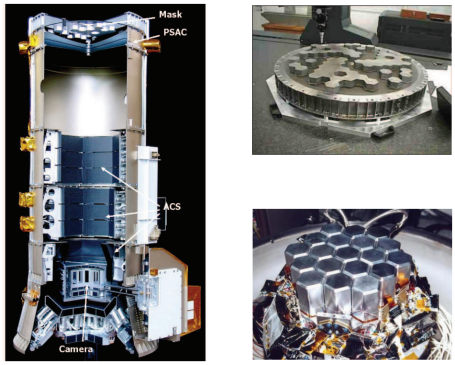

Figure 3.4: Left: A cut-away view of the SPI instrument. Right: view of the coded mask with its tungsten plates and 120 degree rotational symmetry (top) and detector plane with the 19 germanium detectors (bottom). *Source: Dubath et al.[18]*

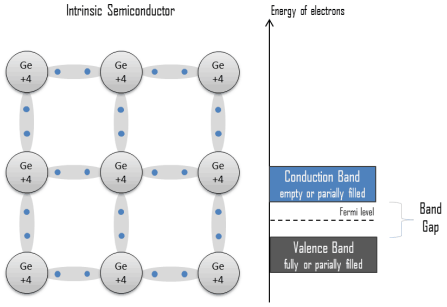

Figure 3.5: Left: Sketch of the crystal lattice of germanium. Right: Diagram of the valence and conduction band in an insulator. *Source:* [5]

In metals there is just no gap, and electrons can jump across with no need for extra energy thus making it electrically conductive. In insulators the band gap is so big, that even with high energy electrons cannot overcome and thus no electric current can pass[3][8]. If outer radiation (e.g. a high energy photon) enters the germanium crystal and interacts with the semiconductor material, it will ionize some of its atoms consequently producing electron-hole-pairs. Of great importance is that the number of electron-hole pairs created is proportional to the energy of the radiation to the semiconductor [5]. Under the influence of an applied voltage, electrons and holes travel to the electrodes, resulting in a pulse that can be measured in an outer circuit. This pulse carries information about the energy of the original incident radiation. The number of such pulses per unit time also gives information about the intensity of the radiation. In our case, the voltage applied is 4kV [27]
With a band gap of ($E_{gap,Ge} = 0.67$ eV) [5], the possibility of thermally excited electrons bridging the gap, proportional to $\exp(\frac{-E_{gap}}{2k_BT})$ [8] can and indeed happens, creating a lot of noise in the final measure. The way SPI overcomes this problem is through active cooling with liquid nitrogen to a temperature of 77K. The reason the detector is made of germanium and not other semiconductors is because of its spectral resolution. Moreover, it can have a sensitive thickness of centimetres, and therefore can be used as a total absorption detector for gamma rays up to a few MeV.

contributing to the electric conductivity.

[3]Completely full and completely empty bands do not contribute to electric conductivity

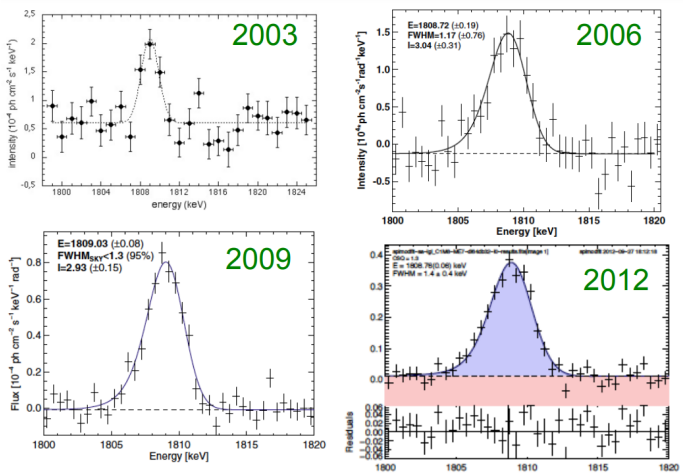

Figure 3.6: The ^{26}Al line measurements with SPI during the INTEGRAL mission. *Source: Diehl et al.* [7]

SPI usually looks at one region of the sky for around 30 minutes getting reoriented by steps of 2.1 degrees around its target. This is called "dithering". These 30 min lapses are called "pointings" which contain both time and coordinate information.

Getting closer to its 20th anniversary, SPI has archieved most of its endeavours. For example, it confirmed the interstellar glow throughout the Galaxy of ^{26}Al GRs early in the INTEGRAL mission, and has been refining those measurements since (see Fig. 3.6). With time, 4 of its germanium detector failed, and the rest began to lose spectral resolution, which was overcame by annealing of the detectors each half year. This is done through a 37-hour long period, where the material gets heated to 103 degrees Celsius. This restores the quality of the crystal lattice, so that charge collection and the original energy resolution is recovered. [13]

CHAPTER 4

Methods

In this section, I will introduce the methods which I used in the analysis of this thesis. I will also describe the process and go deeper into detail in the statistics part.

4.1 Novae Catalogue

Since October 2002 (start of INTEGRAL), 153 novae have been discovered in the Milky Way (although around 1000 were expected). Of these, Siegert et al. [24] have selected 102 for a study of the ^{22}Na line for 16 years of INTEGRAL data, these novae already fulfil some of the criteria for my analysis, so that I will begin with this catalogue. The unfiltered catalogue can be found by clicking here, it consists of 153 Novae with discovery time ranging from as soon as 2002 with the launch of INTEGRAL, to 2018, where I also set the limit for my analysis.
Very important for me were the name, coordinates in galactic system, distance from earth with uncertainties, and exact time of discovery[1] in Modified Julian Day (MJD).

4.2 Pipeline overview

In this section, the standard SPI pipeline is explained. The first program is *"SPISelectScW"*, which takes coordinates of the source and revolutions of INTEGRAL as main parameters and searches in the database if there are corresponding pointings and if the ACS isn't indicating incident cosmic rays. A selection of energies and their binning can be made. Also, a starting and stopping time for the measure can be set, so that the program only looks for data in such time intervals. As output we get a list of Science Windows (ScW) with raw data from the measure.
The next program handles the instrumental background data by *"IDL-Background"*, it builds a background model from the background and response database.
Once the source and background are ready, *"SPIMODFIT"* will use the statistical method Maximum likelihood to fit them into a single function.

[1] Time where the visual peak was measured

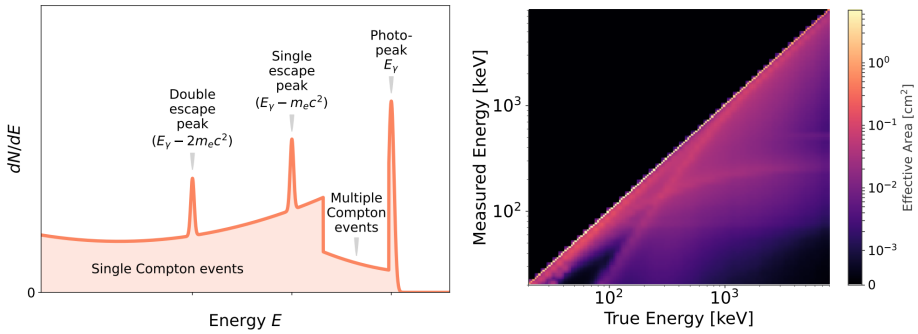

Figure 4.1: Left: Interactions of photons inside the detector. Compton scattering leads to a characteristic continuum below the photo-peak and it can be seen as a faint line away from the main diagonal (Right). Right: Energy dispersion matrix of SPI. The heat-map reflects the probability of a photon with initial energy E_i to be detected at a lower final energy E_f. [22]

The last step is to use the program 3ML to fit our processed spectral data points with a function of interest.

4.3 Pipeline details

Some important terms I will use throughout this section are **"Response"**; this is basically how a photon looks in the sky for our instrument, called data space. This data space can be further divided into 3: abstract, raw and real data space. The first one is spanned by reconstructed or inferred variables, such as the number of detectors in coded mask telescopes like SPI. The real data space of each instrument goes down to the level of its electronics and the specific geometry such as the coding mask of SPI, and it is always one of the many ways to visualise the raw data. In this thesis, the method Forward-modelling will be used, which is the only statistically proper way to analyse GR data [22]. It is used to convolve models with physical units into the raw data space of channel number per detector unit. Taken into account is for example the fact that photons not always deploy all its energy when entering the detector (see Fig. 4.1).
The other terms are **"Sky"** and **"Background"**, by sky I mean the image generated by the source, and by background I mean everything that we measure but is not coming from our source.

4.3.1 Maximum likelihood method

Given a probability model $M(x, \theta)$, and a parameter space Θ, there are several different approaches that can be used to determine an estimator of θ. For instance, the Bayesian method, and the MLE are very well tested approaches. These are both based on the likelihood function $\mathcal{L}(\theta)$, which, for a sample $S = X_1, ..., X_n$ is given by $\mathcal{L}(\theta) = \prod_{i=1}^{n} f(X_i, \theta)$. If the sample S consists only of independent variables, then we get

$$\mathcal{L}(\theta) = \prod_{i=1}^{n} f_i(X_i, \theta) \tag{4.1}$$

This function links the observed data S and the probability model M so that statistical inferences can be made about θ.
As we will see later, it is easier to work with the logarithm of the likelihood $\ell(\theta) = \log \mathcal{L}(\theta)$. This is possible since the natural logarithm is a monotonically rising one-to-one function on $\mathbb{R}^+$ and thus no information about the maximum is lost. Using the properties of the logarithm we get to the equation

$$\ell(\theta) = \log \left[\prod_{i=1}^{n} f_i(X_i, \theta) \right] = \sum_{i=1}^{n} \log f_i(X_i, \theta) \tag{4.2}$$

When $\theta \subset \mathbb{R}$, and the log-likelihood function is differentiable with respect to θ, we can define its first derivative [19].
Now, for the MLE we will use the notation $\mathcal{L}(X|M)$ reads: X given M, in a nutshell it describes the probability of measuring data X when your expectation model is M. So, in case of our photon counting method we ask: how likely is it to measure x counts (per time, per energy bin, per detector) when my model suggests M counts? For it, we want to choose the value of $\theta \subset \Theta$ that maximises the likelihood function. For it, we take the derivative with respect to θ. This value is the one which most agrees with the observed data. In this thesis, I will work with large datasets, and this is the reason why using the logarithm is advantageous. However, the data sample is going to be so large that this problem will not be even analythically solvable. To solve it numerically, *SPIMODFIT*, which will use this method to fit the sky and the background with the response to a single point, will use the Levenberg-Marquadt algorithm.
The model I will be fitting relates all the terms I mentioned earlier into one output:

$$M(p) = \alpha \cdot R_{SKY}(p) + \beta \cdot R_{BG}(p) \tag{4.3}$$

where p is the pointing, R the response functions, and α, β are weighting parameters. The term $\alpha/T_p \cdot A_{eff} = F$, is the flux in units of $\mathrm{ph\,cm^{-2}\,s^{-1}}$ that we are interested in. Since we deal with unit pointings (not changing in time and independent of energy), we absorb the factor $T_p \cdot A_{eff}$, i.e. the observation time per pointing T_p, and the effective area A_{eff} of how much collecting area the instrument actually has for our photons, into the sky response R_{SKY}.
Any counting experiment follows the Poisson distribution[10]

$$P(x|M) = \frac{M^x e^{-M}}{x!} \tag{4.4}$$

so for each pointing p, and with our model M we get:

$$P(x|M) = \frac{(\alpha \cdot R_{SKY}(p) + \beta \cdot R_{BG}(p))^x e^{-(\alpha \cdot R_{SKY}(p) + \beta \cdot R_{BG}(p))}}{x!} \tag{4.5}$$

and thus for the final likelihood function:

$$\mathcal{L}(x|\alpha, \beta) = \prod_{i=1}^{n} \frac{(\alpha \cdot R_{SKY}(p_i) + \beta \cdot R_{BG}(p))^{x_i} e^{-(\alpha \cdot R_{SKY}(p_i) + \beta \cdot R_{BG}(p))}}{x_i!} \tag{4.6}$$

The logarithm of this function is:

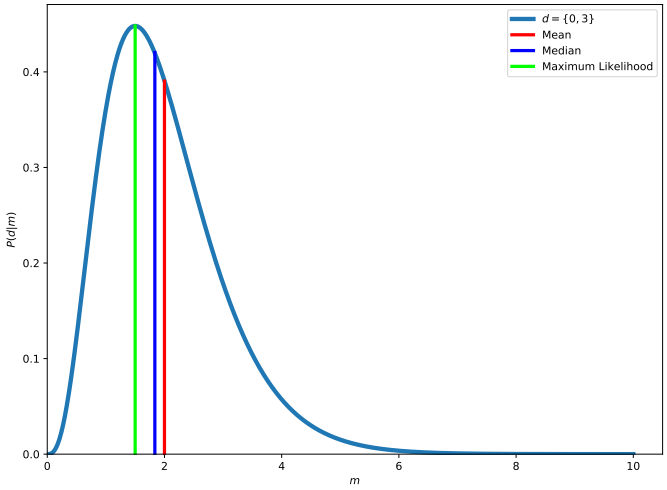

Figure 4.2: Poisson distribution of a dataset with its Mean, Median and Maximum likelihood.

$$\ell(x|\alpha,\beta) = \sum_{i=1}^{n} \frac{(\alpha \cdot R_{SKY}(p_i) + \beta \cdot R_{BG}(p))^{x_i} e^{-(\alpha \cdot R_{SKY}(p_i) + \beta \cdot R_{BG}(p))}}{x_i!} \tag{4.7}$$

this is what *SPIMODFIT* will be maximising.

Chi-squared method and Degrees of Freedom (DoF)

As a measure to assess the goodness of a fit, *SPIMODFIT* will use the Chi-squared function. This is a very popular method for model assessment, model comparison, convergence diagnostic, and error estimation in astronomy.
With a dataset of points (X_i, Y_i) being fitted to a model M with adjustable parameters $\theta_1, ..., \theta_k$, and measured with uncorrelated Gaussian errors σ_i, the function is defined as:

$$\chi^2 = \sum_{i=1}^{n} \left(\frac{Y_i - M(X_i; \theta_1, ..., \theta_k)}{\sigma_i} \right)^2 \tag{4.8}$$

This way, each data point is weighted with its significance. Moreover, if we define the quantity DoF as K, the number of data points minus the number of fitted parameters, we arrive at the so called reduced Chi-squared, widely used in astronomy, which gives us new important information:

$$\chi^2_{red} = \frac{\chi^2}{K} \tag{4.9}$$

This number should be equal to 1 within the Gaussian error $\sigma = n\sqrt{2/K}$, where n is the selected standard deviation; if it is larger we consider it a bad fit, and if it is smaller, it its considered an overfit which is also not good because there are too many parameters for little data samples. [2]

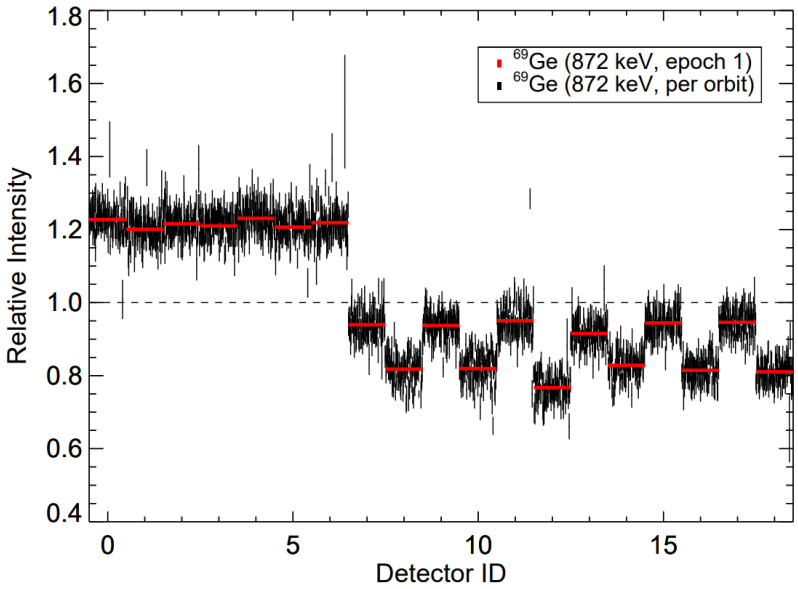

Figure 4.3: Example of instrumental BG radiation. The line at 872 keV from ^{69}Ge reveals a pattern in the measurements; the inner Germanium detectors measure more than the outer ones. See Fig. 3.3 for detector ID numbering. [6]

4.3.2 Background modelling

Instrumental background (BG) radiation dominates in our energy regime. A method to model the BG is very difficult to establish for such a telescope in a space environment where the sun's activity changes over time, as well as the germanium detector's spectral resolution degrades over time. The main part of the BG comes from nuclear de-excitation reactions and continuum processes, such as bremsstrahlung, of the instrument and satellite material, being exposed to cosmic-rays (see Fig. 4.3). Siegert et al. [23] developed a very robust model applicable for SPI, which makes use of the spectral background and response database (SBGRDB, Diehl et al. 2018 [6]) and divides, for each specific energy, the model in two components: photons from continuum processes such as electron-positron-annihilation, and photons from GR-lines producing processes such as beta-decay. These two individual models will get weighted differently according to the energy, and discriminate between processes happening outside the detector, which will influence the pattern cast onto it in dependence of each pointing, and processes inside the detector, which do not influence the patterns, but only the amplitude. The model takes care of the solar activity as well as instrument degradation, and is shown to be reproducible and delivering values from celestial sources in concordance with the literature.

4.3.3 Spectral analysis

So now we have a set of fitted points which have energy on the x-axis and flux on the y-axis. The next question is if they follow a specific spectral model or are consistent with zero. The way I will do this is by using Bayesian Estimation (BE), which works similarly to the MLE but with a key difference; we allow our model to change according to the data sample. This way we keep updating our model as it obtains information from the data until we get a very robust result.
In BE, the value of θ in our model $M(x, \theta)$ is a random variable having its own

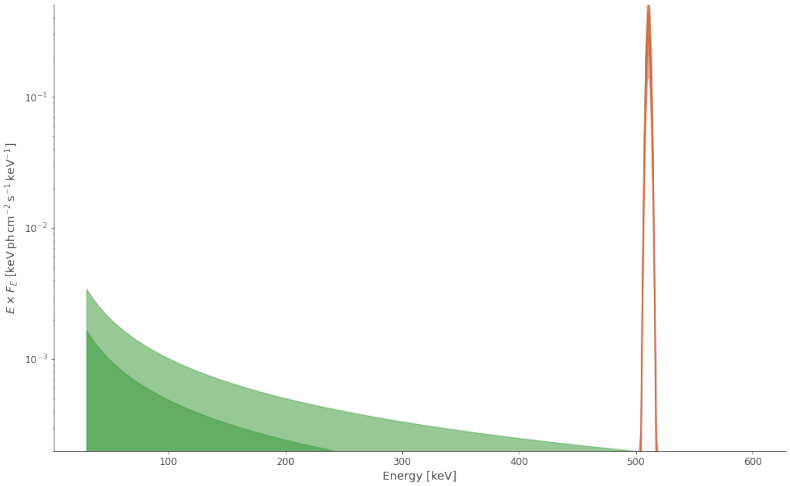

Figure 4.4: Power-law (green) plus Gaussian (orange) curve. The different shades reflect the standard deviation from the mean.

Probability Density Function)[2] (PDF called the *prior distribution*. It is based on the possible values of θ in the parametric model and reflects the uncertainty of θ before the data has been collected. Here we get to choose the prior based on information (or lack of) about θ. We just need to be sure that we don't rule out possible outcomes by choosing very objective or specific priors. Having now information both coming from the priors and the sample, θ will be estimated using them. From now on, the PDF of our parametric model will be denoted as $M(x|\theta)$ rather than $M(x, \theta)$ since we have a conditional distribution.
Inferences about θ in the Bayesian approach are based on the distribution of θ given the observed values of a random sample $x = x_1, ..., x_n$ which is called the *posterior distribution* and is denoted by $M(\theta|x)$. It is determined by Bayes Theorem as follows:

$$M(\theta|x) = \frac{M(x|\theta)\pi(\theta)}{\sum_{\theta\in\Theta} M(x|\theta)\pi(\theta)d\theta} \tag{4.10}$$

with $\pi(\theta)$ the prior distribution.
This posterior distribution combines the information about θ in the prior distribution and the likelihood function to produce an updated distribution containing all of the available information on θ.[19]
In this thesis, I will be using two models to fit the spectra.

Empirical model

The first model only uses the SE section of SPI and is a linear combination of two functions; a Power-law and a Gaussian. The Power-law accounts for the low-energy regime, here we expect greater fluxes as we approach the lowest energy measured (20 keV). The Gaussian, on the other hand, accounts for the 511 keV line, it is centred exactly at that point with a standard deviation of 1.7σ. The amplitude K of this function which represents the flux F in units of ph cm^{-2} s^{-1} is what I will be looking at since it reflects the significance of detecting a CNe (see Theory).

[2] A statistical measure used to gauge the likely outcome of a discrete value

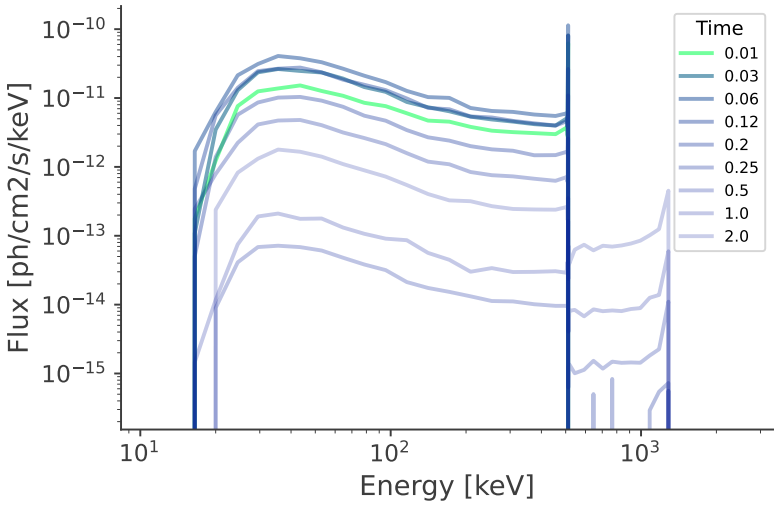

Figure 4.5: Example of a Table model of a ONe CNe with a mass of $1.2M_{\odot}$ at a distance of 1 kpc, taken from Leung and Siegert [14] at different times. The 2 characteristic lines at 511 keV and 1275 keV are visible, as well as the continuum, product of positronium decay and Comptonized 511 keV.

Astrophysical model

These models are taken from CNe simulations made by Siegert and Leung [14], and by Hernanz [11]. They are not functions but a template of energy bins and fluxes (exactly like our data points) and are much more complex than the first model. Here they account not only for the characteristic lines like the 511 keV and 1275 keV but also for the continuum these lines leave behind them, that come from positronium decay and 511 keV photons undergoing Compton scattering. They use both the SE and PSD region. Here I will be fitting the amplitude K of the whole function, which represents the flux throughout the energies, and checking its significance. As these simulations have also a time dimension (see Fig 4.5), I will be fixing the time at the point of maximum global flux, because there is where our instrument has the greatest chance of measuring something.

CHAPTER 5

Results and Discussion

5.1 Catalogue

As mentioned in section 4.1, Siegert et al. [24] already did filtering to the 153 novae, their eligibility criteria required novae to be no further away than 25 kpc (inside the Milky Way) and to be CNe[1]. Nevertheless, not all of them are eligible for my search for the 511 keV line, since that happens before the visual discovery, and INTEGRAL can therefore only have looked at the source by chance. The first filter I applied was regarding our instrument: only those CNe which were observed within a 10 by 10-degree field of view[2] by SPI in a time window of 14 days before the visual peak was measured on earth passed through. The number of candidates was further reduced to 41. Subsequently, other selection criteria were used such as SPI being outside the Van Allen radiation belts, no cosmic rays indicated by the ACS, and radiation monitors indicating nominal values. The final number of CNe came down to 36. The results are shown in table 5.1.

5.1.1 Selecting the Science Window (ScW)

From the Theory, we know that GRs coming from CNe have a characteristic spectrum, and reach a peak for only a short period to vanish again. The first reasonable thing to do is to separate and select the active energy bins of our instrument according to what we expect. In my case, I left a dedicated bin for the 511 keV line (from 508-514 keV) and for the 1275 keV line (from 1265-1285 keV) knowing these are the energies at which I have the greatest chance of measuring something (see Fig. 4.5). For the remaining bins, I made a logarithmic spacing (the greater the energy, the greater the energy bin).
I also get to insert a starting and stopping time for my measure. If I were to take the whole 14-day measure (or the time SPI managed to measure within these 14 days) and analyse it, I would get a horizontal line when checking for the flux at both

[1] By taking faster recurrent novae, noise in the measures from earlier outbursts would have to be taken care of

[2] So that they are not at the edge of exposure

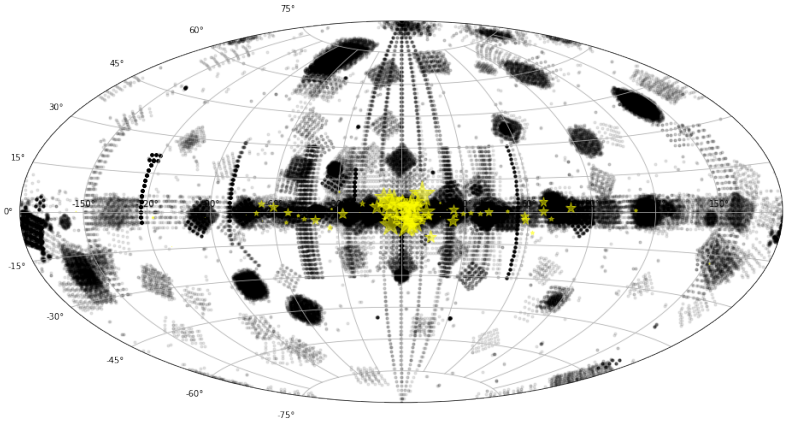

Figure 5.1: Places in the sky where INTEGRAL already looked at are marked from white (never looked) to black (long times of exposure). The novae are also marked in the diagram with a star, the bigger the star, the longer it was observed. All novae lie in the galactic plane (horizontal axis) and most of them are in the centre of our galaxy.

dedicated energy bins. This is not what I want, as the mean flux is not what I am interested in, but the instant flux. The manner I approached this was by defining a time-resolution of at least 1 hr and at most 2 hrs. If a pointing was not long enough, then I would append the next one, and so on, until my time-resolution was reached. If there was a gap of more than 5 hours between two pointings, I prioritised longer (but with pointings back-to-back) time-windows over "fake" measurements (with pointings being spread over 5 hours or more) of several hours. This way I had both time- and energy-resolved data prepared for further analysis.

5.1.2 Creating Spectra

Next I ran *IDL-Background* and *SPIMODFIT* to create the spectra. Important for me was that $\chi^2_{red} = 1$ within standard deviation of 3σ (see section 4.3.1). This meant the Fit worked and I can trust the data. Roughly 1 in 50 time-windows exhibited a very high χ^2_{red} from 20 to around 100 keV, so that I couldn't work with this data, the Bayesian Fit began therefore at 100 keV. Moreover, and for reasons I don't know, about 1 in 100 time-windows had their data not fitted at all by *SPIMODFIT* and had to be completely discarded. Nevertheless I had plenty of data to fit to my models in the next step.

5.2 Search for 511 keV emission

Starting with the 36 CNe with each of them having anything from 30 to 100 time-windows worth of spectra, the next phase was to fit each of these time-windows with a model using Bayesian analysis. In the first model I suggested a Power-law plus a Gaussian centred at 511 keV, where the electron-positron annihilation peak happens, with a standard deviation of 1.7σ which is based on the narrow-line sensitivity of SPI of 3σ in 1×10^6 s at 511 keV. Once all Fits were done, spectra[3] for each time-

[3]Flux plotted against Energy

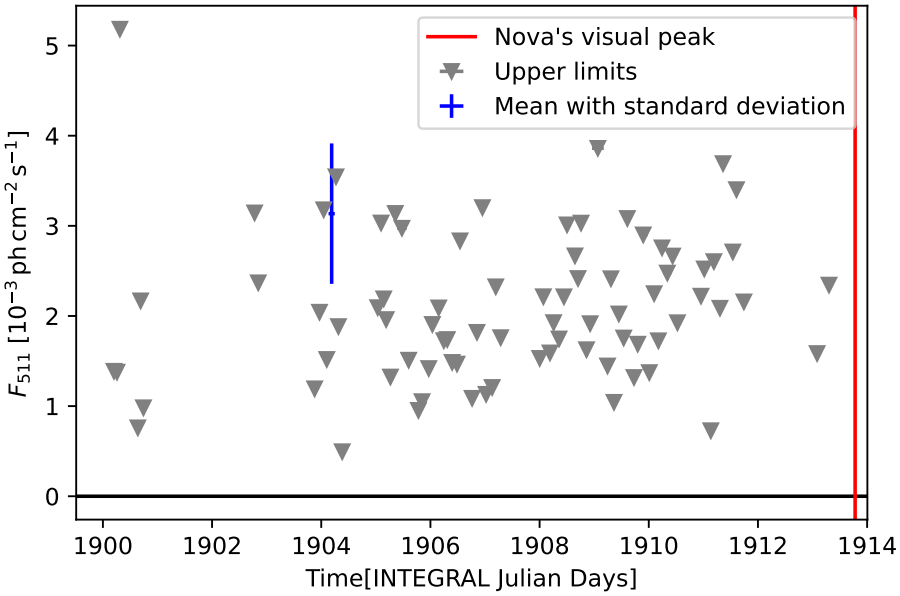

Figure 5.2: Light-curve for the CN V5115 Sgr fitted with the empirical model. In grey are the upper limits represented whose fluxes are consistent with zero. In blue, the only significant measurement. To help the viewer, there is a horizontal line at 0 which represents no flux. Also, the time at which the nova was detected can be seen as a vertical red line. The time is given in INTEGRAL Julian Day (IJD), which began the 1st of January of the year 2000.

window and a light-curve[4] for each CN was created.
Most CNe were either too far away or too dim for our instrument, resulting in significances of no more than 2σ [5]. However, some of them got close to 3σ and only one, V5115 Sgr had a significance of 4σ.

5.2.1 V5115 Sgr

I detected the maximum flux in the time window of 1904.134−1904.248 IJD, translating to around 2 hours and 44 minutes, and happening 9.5 days before the visual peak was measured. The expected peak fluxes from Hernanz's work are in the order of $1 \times 10^{-2}\,\mathrm{ph\,cm^{-2}\,s^{-1}}$ [12] for a CO CNe with a progenitor's mass of $1.15 M_{\odot}$ at a distance of 1 kpc. At its peak, V5115 Sgr exhibited fluxes of $3.1(8) \times 10^{-3}\,\mathrm{ph\,cm^{-2}\,s^{-1}}$ which would hint to similar parameters, if the theory is correct. From Leung and Siegert [14], the expected maximum flux is in the order of $1 \times 10^{-9}\,\mathrm{ph\,cm^{-2}\,s^{-1}}$ for a CO CN with a WD mass of $1.20 M_{\odot}$ also at a distance of 1 kpc. This shows a big discrepancy both to Hernanz model and the flux I measured from the nova. This would either mean that the theory is missing something, or that my measure is not coming from the nova but another source.
Because of the nature of the light-curve, we can be sure that the source peaked for

[4] Flux plotted against time

[5] 4.5% chance of falling outside of the null hypothesis, in this case being to measure no flux. Convention in the scientific world is at least 5σ or around 0.00006% chance of falling outside of the null hypothesis, to be claimed as discovery.

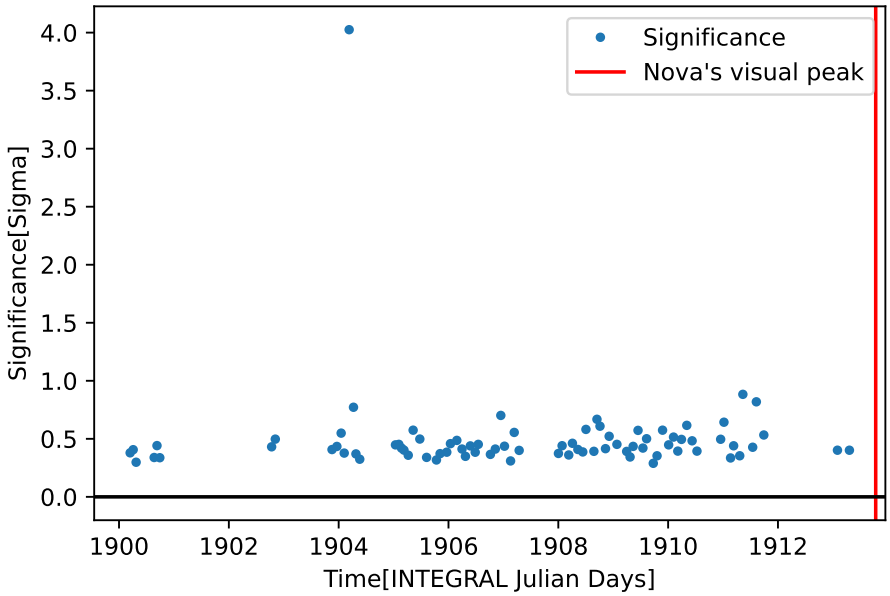

Figure 5.3: Significance of the CN V5115 Sgr fitted with the empirical model. Consistent with the light-curve, the highest significance reached was 4σ. All other points a dispersed at around 0.4σ.

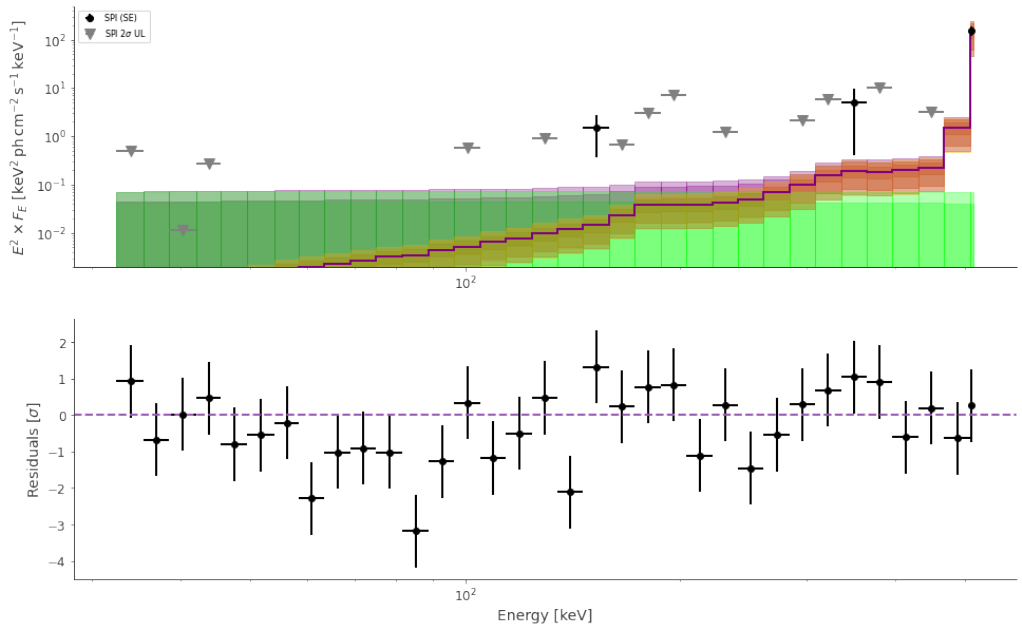

Figure 5.4: Spectrum of the CN V5115 Sgr fitted with the empirical model. In green is the Power-law represented, in orange is the Gaussian curve centred at 511 keV, and in violet is the linear combination of both. The different shades represent standard deviations from the mean. Black points are significant, while grey arrows represent the upper limits. The plot is double-logarithmic, and the flux is multiplied by the energies squared. Also, in the lower plot are the residuals of each data point represented.

only a couple of hours and then returned to a flux consistent with zero. This rules out several non-transient events which would have a constant flux.
As shown in Table 5.1, the estimated distance of nova V5115 Sgr is of 3(1) kpc taken from the work of Özdönmez et al. [17], this is relatively close to Earth, but certainly not the closest; for instance, V5113 Sgr, V5117 Sgr, V2674 Oph, and V5668 Sgr are at a distance of around 1 kpc and yet none of them exhibited any significance in flux. Both from Hachisu and Kato [9] and Shara et al. [21] we get the WD mass of V5115 Sgr to be $1.2(1)M_{\odot}$, taken from a best-fit line of the visual magnitude plotted against the days after outburst, suggesting a ONe CN. Here, the neon content is of 0.03 times its mass, and CNO content of 0.10 times the WD mass. Sadly the masses of the closer novae are unknown so I cannot draw any conclusions from them.
As seen in the light-curves from all measured CNe shown in the appendix, all of them show coverage gaps from SPI. This is because not only is SPI coverage not continuous, but it also varies both in effective exposure and in the observing sequence from one source to another. This means that the peak of the expected GR flux of a nova could be easily missed during such a coverage gap, thus showing no significance in fluxes although the CN is very close to us or has a big WD mass. Moreover, because this peak in flux happens at an unknown time within the 14-day window before the visual detection, one can only talk about the probability that the emission would have been detected.

5.3 Search for broadband emission

As for the broadband, I suggested two models, one taken from Fig. 4.5 at time $t = 0.06$ days (peak luminosity) and the other one from Hernanz also at peak luminosity, in this case being $t = 0.12$ days. Similarly were most CNe of low significance, but this time 3 of them passed the 3σ barrier. V5581 Sgr showed 4.2σ, V5113 Sgr and V382 Nor exhibited 3.6σ and 4.7σ respectively, these last two having also another time-window with high significance back-to-back thus making the measure even more significant. I must remark, that all high significances came from Hernanz's model, which can be explained by the higher expected fluxes.

5.3.1 V382 Nor

This nova shows two peaks in fluxes: two back-to-back in a time window of 1893.491−1893.662 IJD, translating to 4 hours, happening 4.6 days before the visual discovery, and a single, but slightly greater peak in a time window of $1893.877 - 1893.962$ IJD meaning 2 hours, and happening 4.4 days before detection. The peaks are of $3.3(8) \times 10^{-3}\,\mathrm{ph\,cm^{-2}\,s^{-1}}$ and $3.5(8) \times 10^{-3}\,\mathrm{ph\,cm^{-2}\,s^{-1}}$ being again comparable to Hernanz model. Doing Gaussian propagation to the back-to-back fluxes results in a significance of 5.01σ. The distance of 4.0(5) kpc is also taken from Özdönmez et al. [17]. The progenitor's mass is estimated to be $1.2(1)M_{\odot}$ [9], and it is believed to be a Fe II Type CN based on its spectral type [28]. This element comes from the secondary star which later mixes with the WD.
From the light-curve we can also see the peaks, having consistent with zero fluxes in between. This could mean that for some reason, the radiation coming at that time did not manage to get to our detector. This can be sustained by the fact that the

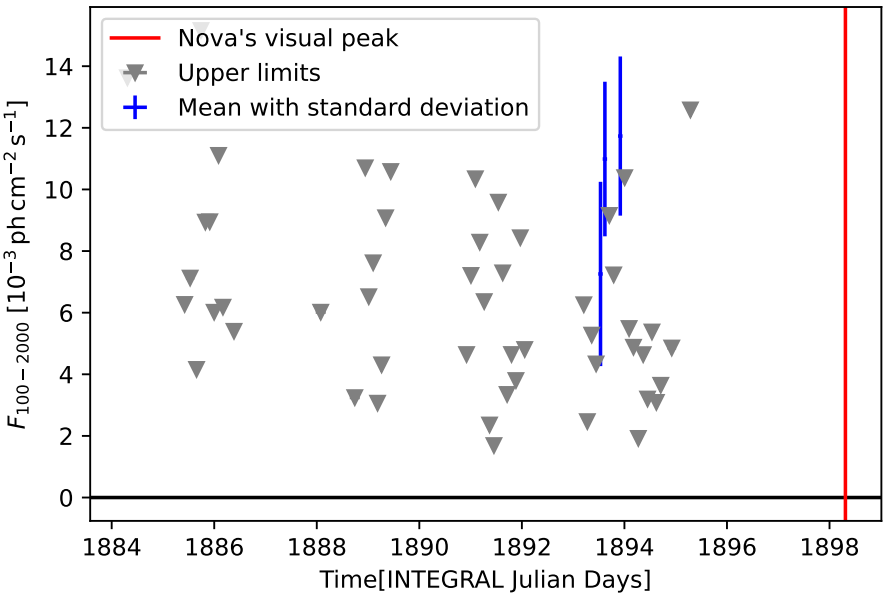

Figure 5.5: Light-curve for the CN V382 Nor fitted with the astrophysical model. In grey are again the upper limits, in blue the significant measurements. In this case, 3 time windows are packed close together. The time at which the nova was detected can be seen as a vertical red line.

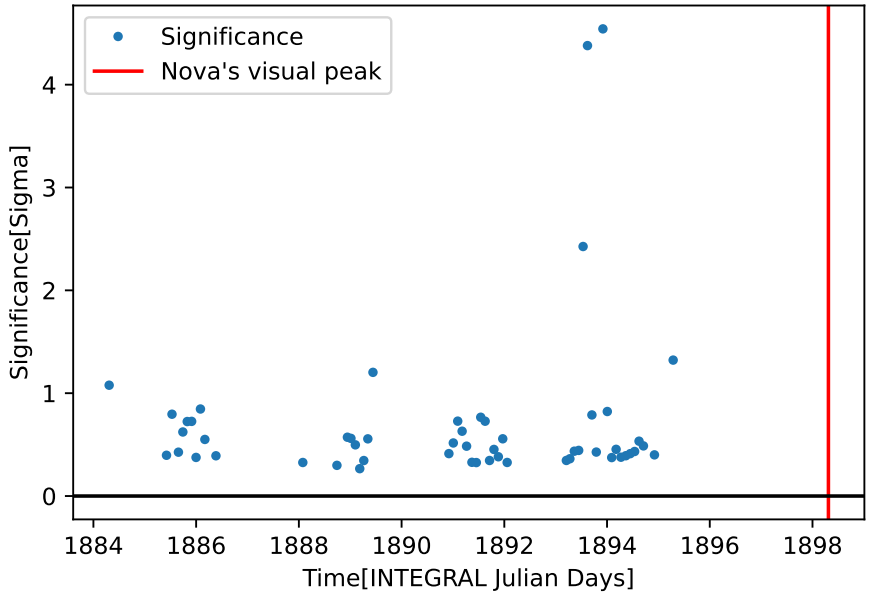

Figure 5.6: Significance of the CN V382 Nor fitted with the astrophysical model. Consistent with the light-curve, the highest significance reached was 4σ. All other points a dispersed at around 0.4σ.

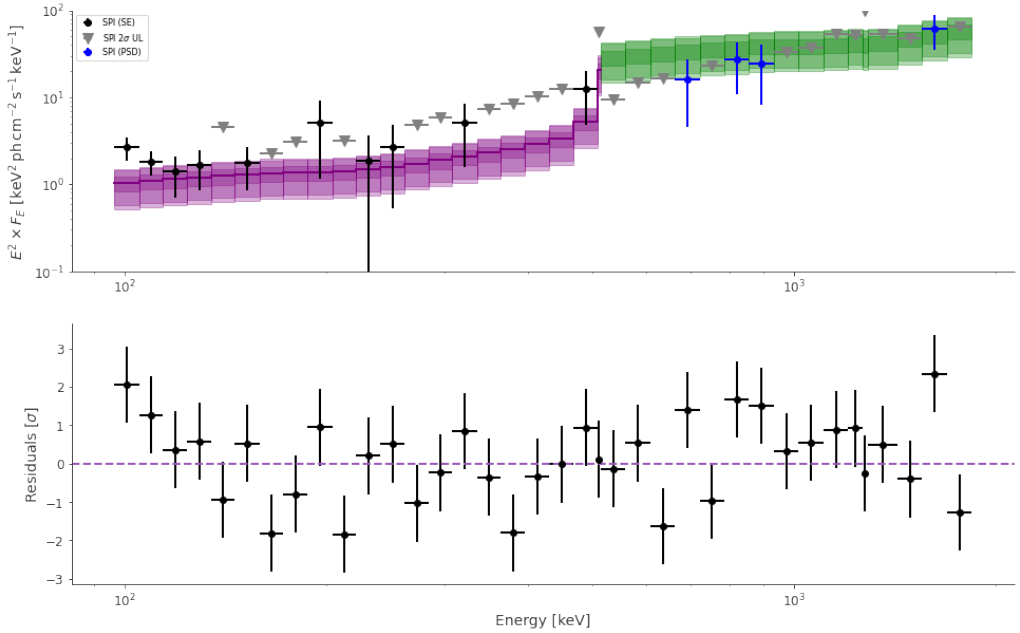

Figure 5.7: Spectrum of the CN V382 Nor. Also a double-logarithmic plot, with the flux being multiplied to the energy squared. In purple is the SE region of SPI, and in green the PSD region. Black points refer to high significance in the SE region, and blue points refer to high significances in the PSD region. Grey points represent upper limits.

peaks are only 5 hours apart.

When looking at the light-curves of significant CNe fitted with the empirical and astrophysical model, a time correlation cannot be seen. When one CN exhibited high fluxes with one model, it did not the same with the other and vice-versa. However, the nova V5113 Sgr showed some significance at close time windows in relation to the astrophysical model, as seen in Fig. 5.8. Because the peaks happen one day apart, it is not very plausible that they originated from the same event.

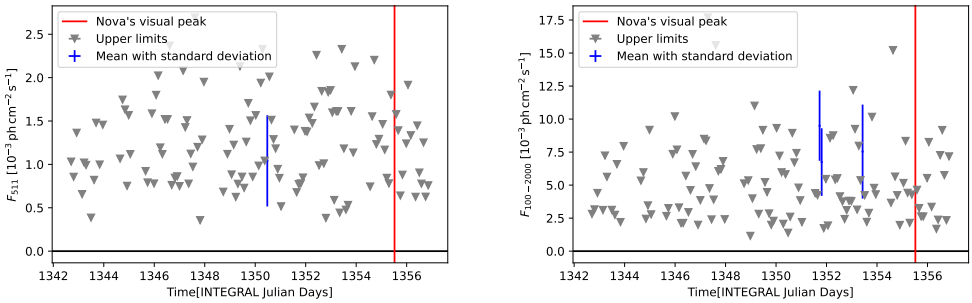

Figure 5.8: Left: Lightcurve of the Nova V5113 Sgr with the empirical model. Right: Lightcurve of the same nova, with the astrophysical model. As seen in blue, the greatest significance of high flux at the 511 keV line happens about one day before the highest flux in the broad band is measured. This is somewhat plausible, since the 511 keV line is more energetic and thus can get through envelope of the CNe and the universe more easily, arriving sooner at the Earth. However, 24 hours is too much apart for an event happening only 1 kpc away.

5.4 Comparison with IBIS

To cross-check my results, I used the imager on board INTEGRAL IBIS, mentioned in section 3.1, which is coaligned with SPI and thus always points in the same direction. The interface to the instrument MMODA was kindly provided by the team of Neronov et al. [16] with support from the University of Geneva. I looked at the spectra of the 4 significant CNe at the time where they had their peak in flux. Also, because IBIS is more sensitive in this energy regime, the continuum behind the 511 keV line should generally be more detailed. This is because its maximum effective area lies between 200 and 400 keV for single events, making it more sensitive than SPI below 300 keV. From 300 to 400 keV are they about equally sensitive, and above that is SPI more sensitive.
After spectra in the range 28-514 keV from the novae at the time window of peak flux was gathered, as well as one time window before and one after the peak, I analysed the data with 3ML using Bayesian analysis as I did with SPI. The measurements resulted in detailed spectra and short light-curves, which did not show any significance for any of the CNe this time.

Also, using MMODA I generated images in the GR spectrum, at the time where the novae exhibited their highest peaks. The images span the energies 30 keV to 100 keV, where the continuum should be visible. Also in this case, no significantly bright spots were found where the CN should have taken place (see Fig. 5.10).

Having now both data from SPI and IBIS, to make a fair comparison between them I need to derive the fluxes for each one in the unit erg cm^{-2} s^{-1}. This is done through a convolution between the spectrum and the response of each detector. The erg is a unit for energy, and it is defined as 1 erg = 1 µJ = 1 cm^2 g s^{-2}. After the fluxes were derived, the highest flux measured by SPI for each of the 4 significant CNe was compared with the upper bound determined by IBIS, the results are presented in table 5.2.

From this table, the SPI measurements lose credibility, since they lie well above

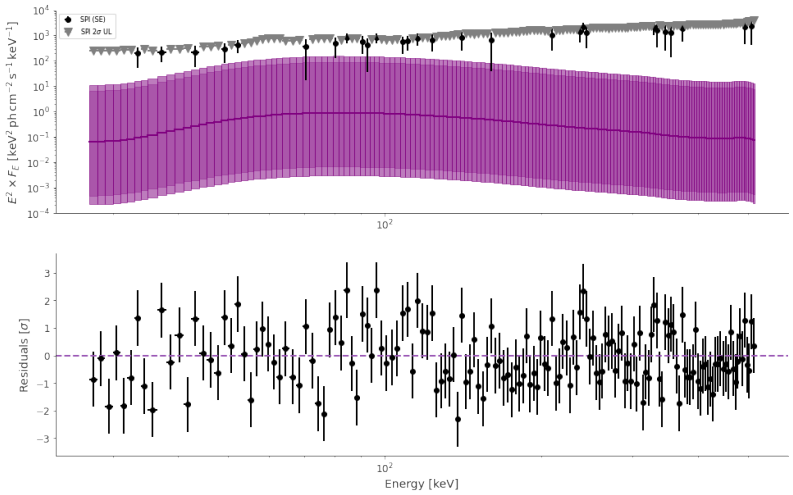

Figure 5.9: Spectrum of the CNe V382 Nor using the imager IBIS. As mentioned, much more detail can be seen in this energy regime compared to SPI. In purple is the mean model in data space, and its shades represent standard deviations from the mean. Grey arrows represent upper limits, and black points represent significant measurements, together with its uncertainties. The lower plot shows again the residuals, left after fitting the measurements to the model.

the upper bounds coming from IBIS. The next question is why SPI measured such high fluxes, when IBIS restricts the highest possible flux to be below these measurements. A possible reason are reactions inside SPI's detector which were not taken into account, or just a statistical high significance which can be expected when measuring and fitting so many points. For instance, 3σ significances will appear about once every 370 measurements, and 4σ significances around 1 in 16000. Estimating all my measurements[6] to be in the order of 4000, the maximum reasonable significance expected would be around 3.5σ. The 5σ measurement from V382 Nor can clearly not be an outlier -2 million time-windows would have had to be analysed for such an event.

[6]Time-windows, for each the spectra was fitted.

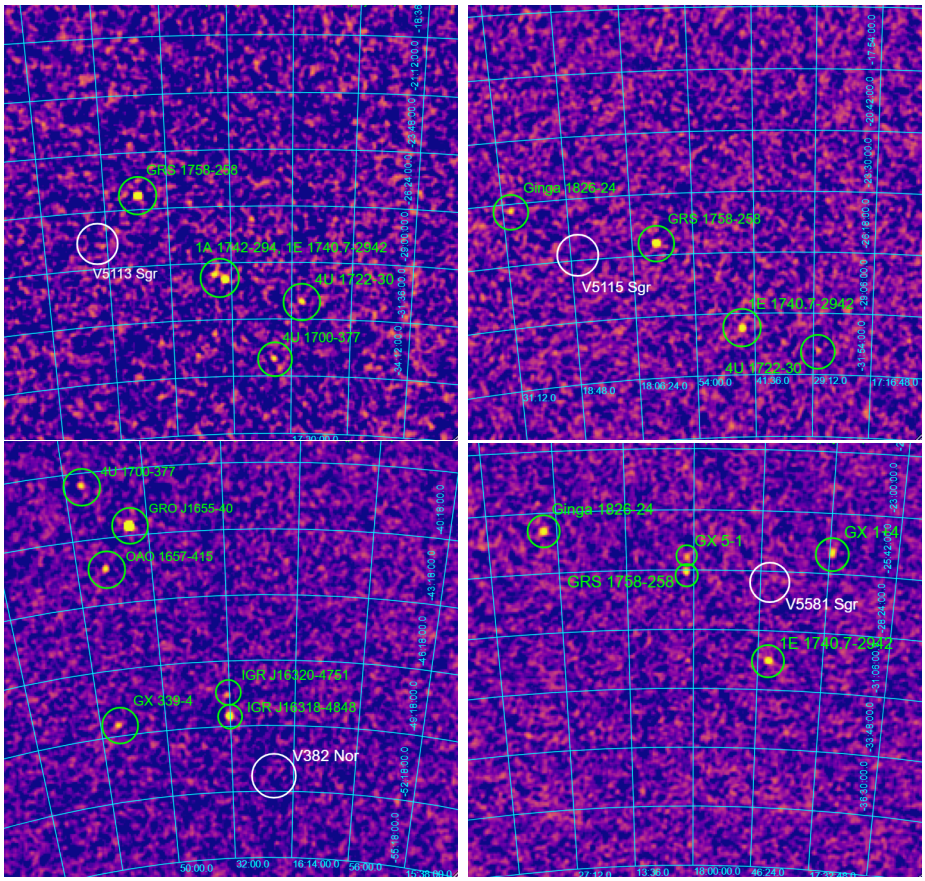

Figure 5.10: IBIS images from the significant CNe. Upper left: V5113 Sgr (time-window 1351.68-1351.85 IJD), upper right: V5115 Sgr (time-window 1904.134-1904.248 IJD), lower left: V382 Nor (time-window 1893.4-1893.97 IJD), lower right: V5581 Sgr (time-window 3387.52-3387.64 IJD). The chosen colormap does not reflect the wavelength, but the magnitude of the source (the closer to yellow, the brighter the object). In sky-blue is the ICRS coordinate grid represented. In green, bright known sources, which were taken into account. In white, the place at which the CN was expected. The energy selected is 30-100 keV.

Discussion

This work used robust methods throughout, some of them very well tested like *SPIMODFIT* or 3ML. The generated catalogue was double checked with several peer-reviewed articles and atlas. *IDL-Background* is also shown to work, and deliver stable results, so that I can be sure that the pipeline can be trusted. The priors suggested in the Bayesian analysis were very uninformative, taking biased assumptions out of the equation. Nevertheless, the expected GR flux from a nova depends critically on nuclear reactions rates which are still uncertain. In this case, the work from Leung and Siegert [14] was taken into account but other previous models like Hernanz [12] are just as valuable.

Although not confirmed by the correlation between broadband emission and the 511 keV line, and the cross-checking with the IBIS instrument did not result in a success, the possibility of a CN measurement cannot be ruled out. The sensibility of these telescopes is not enough for clear proof yet, so that this retrospective analysis

cannot claim a discovery.
As this work relies solely on old data which was not gathered with the intention to measure GR flashes from CNe, the resources are limited. Coverage gaps were present even in the sources where INTEGRAL was looking at by chance, making a full analysis impossible.
However, some things can be changed to have a greater chance of claiming a discovery. For instance, I fitted the Sky and Background separately, but a program that can do them simultaneously is currently under development, called PySPI. Such a fitting could improve the sensibility even further, so that the CNe with high significances measured in this work can be re-analysed in the hope to confirm my findings. Also, INTEGRAL is still active, and the possibility of deliberately targeting future CNe is not small, considering what we know. Recurrent novae have a relatively constant period which can be used to predict when the same nova will explode so that INTEGRAL can already be looking there. Also, despite low, the possibility of detecting a nearby nova must be considered since the information that could be obtained would be of enormous value. Such a source might be detectable by the on-board software even if the optical peak has not been seen on Earth (might as well never be seen given that interstellar dust blocks light, but hardly affect GRs), triggering the spacecraft to bring its position to that direction and measuring spectra.

Table 5.1: Final catalogue for the analysis. A total of 36 CNe from 2002 to 2018 passed all filters. Coordinates are given in the galactic system, revolutions refer to the first and last revolution SPI has gathered data from the CNe in the selected time window. The discovery date can also be found, given in INTEGRAL Julian Day, as well as the distance from earth together with its uncertainty. Of many CNe the distance could not yet be calculated, these are marked with the distance 8.179 kpc which is our distance to the centre of the Milky Way subjected to the uncertainty of double this length, hinting that we only know it is in our galaxy.

Name	Lon (deg)	Lat (deg)	Dist (kpc)	Found (IJD)	Revolutions
V5113 Sgr	3.7	−4.1	1.0(2)	1355.52	109−113
V382 Nor	−27.7	−1.0	4.0(5)	1898.31	290−293
V5115 Sgr	6.0	−4.6	3(1)	1913.78	295−299
V5117 Sgr	−5.4	−6.4	1.5(3)	2239.37	406−408
V2576 Oph	−3.8	5.4	2(1)	2287.57	421−425
V1065 Cen	−66.0	3.6	3.3(5)	2579.35	518
V2615 Oph	4.1	3.3	2.1(8)	2634.81	536−540
V5558 Sgr	11.6	0.2	2.1(4)	2660.78	545−547
V5579 Sgr	3.7	−3.0	13(6)	3030.78	668−673
V1212 Cen	−46.1	−3.5	8.179	3160.05	712−716
V1721 Aql	41.0	−0.1	8(2)	3187.50	722−726
V5582 Sgr	7.5	4.7	8.179	3341.95	776−777
V5581 Sgr	2.3	1.8	8.179	3398.68	791−795
V496 Sct	25.3	−1.8	3.2(8)	3568.37	848−852
V2674 Oph	−2.2	3.6	1.7(4)	3701.85	895−897
V1310 Sco	−11.5	2.2	8.179	3703.86	895−898
V5586 Sgr	1.5	−1.0	8.179	3765.78	914−918
V5588 Sgr	7.8	−1.9	3.1(7)	4103.83	1028−1032
V1313 Sco	−18.4	3.8	8.179	4266.37	1081−1083
V2676 Oph	0.3	5.3	8.179	4467.79	1149−1153
V1724 Aql	32.8	−0.4	8.179	4676.44	1219
V5668 Sgr	5.4	−9.9	1.5(7)	5552.63	1513−1517
V2944 Oph	6.6	8.6	8.179	5566.77	1519−1522
V2949 Oph	2.8	4.6	8.179	5762.41	1592−1595
V5850 Sgr	12.6	−2.6	8.179	5782.38	1603−1604
V555 Nor	−33.1	1.6	8.179	5911.35	1650−1651
V1656 Sco	−5.2	2.5	8.179	6093.48	1716−1721
V1659 Sco	−4.1	−1.9	8.179	6094.00	1717−1722
V5855 Sgr	4.0	−4.0	13(6)	6137.38	1734−1738
V5856 Sgr	4.3	−6.5	8(4)	6142.02	1735−1740
V1660 Sco	−3.6	1.6	8.179	6496.00	1871−1872
V357 Mus	−65.7	−4.1	8.179	6588.49	1903−1907
FM Cir	−51.2	−5.3	8.179	6593.71	1905−1907
V1663 Sco	−12.6	1.9	8.179	6629.36	1918−1923
V3665 Oph	−3.7	5.8	8.179	6643.81	1923−1926
V5857 Sgr	11.5	1.8	8.179	6672.72	1937−1939

Table 5.2: Flux comparison between SPI and IBIS for the 4 significant CNe. The type of model used can also be seen, astro meaning the astrophysical model and empiric meaning the empirical model. The energy range for which the flux was calculated is also given, being 100 to 300 keV for the astrophysical model and 507 to 514 for the empirical model. The column for flux represents the measurement from SPI, which exhibited the high significance, while the column for upper bound (UB) represents the inference for IBIS's measurement, once I analysed the same data I did for SPI. The n before erg stands for nano (10^{-9}). As seen, all upper bounds determined from IBIS lie below the fluxes measured from SPI.

Nova	Model	Energy range (keV)	Flux ($\mathrm{nerg\,cm^{-2}\,s^{-1}}$)	UB ($\mathrm{nerg\,cm^{-2}\,s^{-1}}$)
V5113 Sgr	Astro	100−300	2.0	0.02
V382 Nor	Astro	100−300	2.3	0.01
V5115 Sgr	Empiric	507−514	2.5	0.18
V5581 Sgr	Astro	100−300	2.0	0.12

CHAPTER 6

Conclusion

In this work, high significances reaching 5σ of GR flashes coming from CNe were measured, showing evidence that GR do leave the nova while it is transparent to them. A cross-checking with IBIS challenged these measurements, delivering upper bounds lower than the fluxes determined with SPI. Some possible reasons for a false positive were cited, but a true positive cannot be completely refuted. Further studies with newer software (best-case scenario also with new hardware) will have to be carried out for a confirmation. The paradigm that gamma-rays were never measured coming from a nova is still standing, but this time it has been seriously challenged.

APPENDIX A

Appendix

Animation of V382 Nor

Animation of the CN V382 Nor from 1893 to 1894 IJD (where the highest flux was observed) in steps of 0.1 days. The instrument used is IBIS on board of INTEGRAL, the energy range is 30-100 keV. (Must have Adobe Flash to see it)

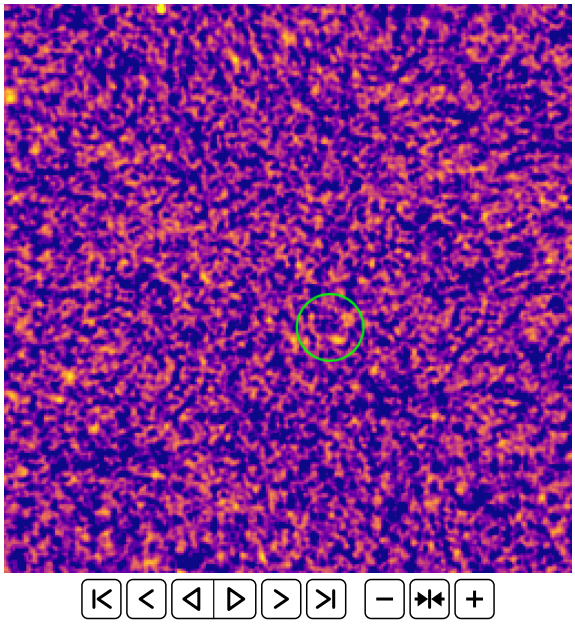

Lightcurves from all analysed CNe

Generated the same way as Fig. 5.5, below a significance of 2σ, only the upper bounds are shown.

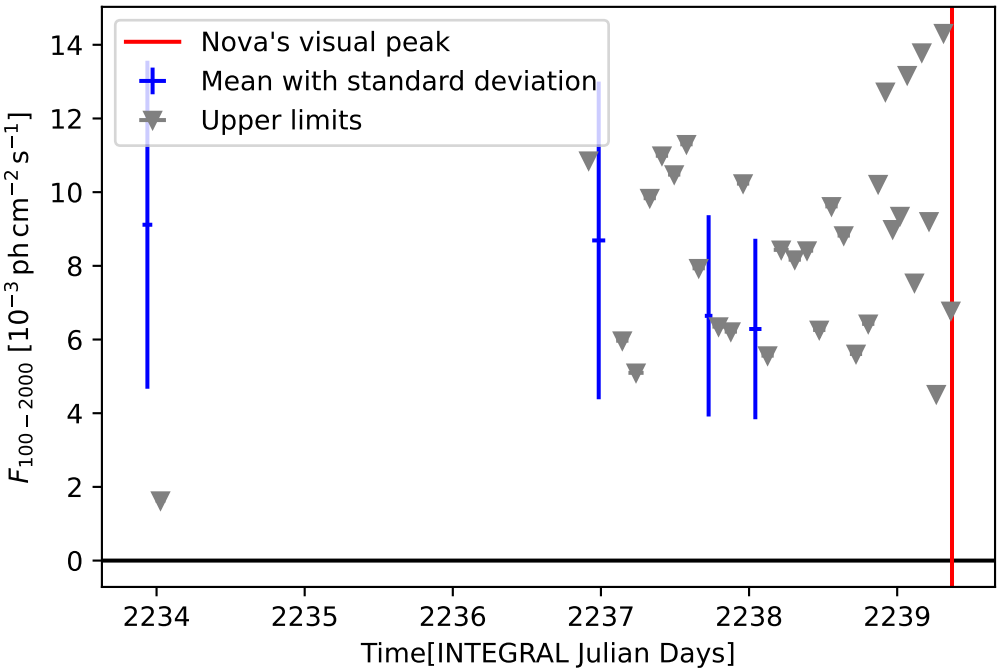

Figure A.1: Lightcurve of V5117 Sgr

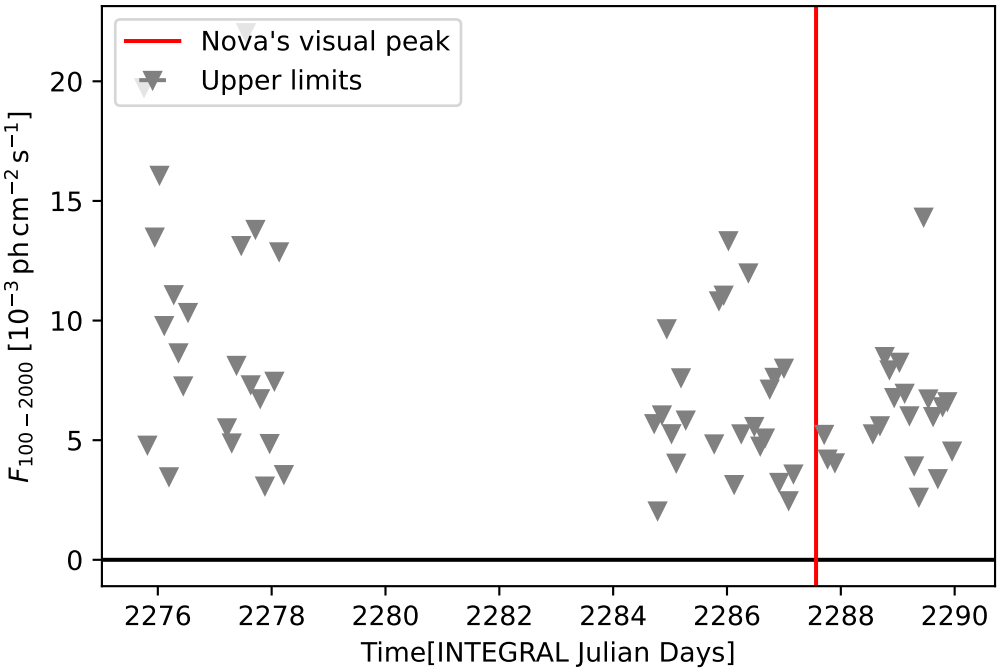

Figure A.2: Lightcurve of V2576 Oph

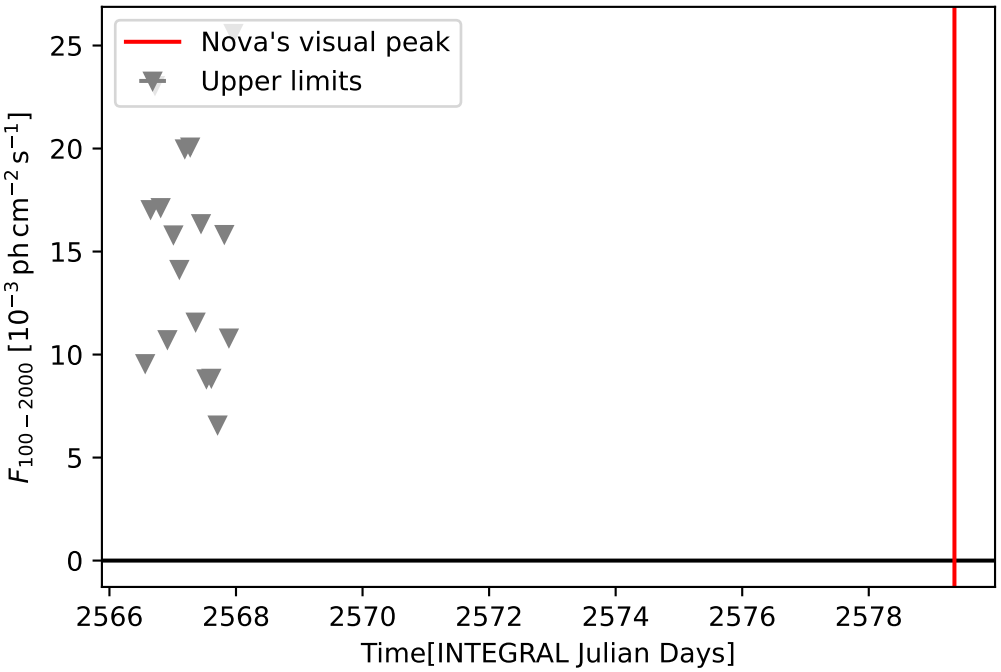

Figure A.3: Lightcurve of V1065 Cen

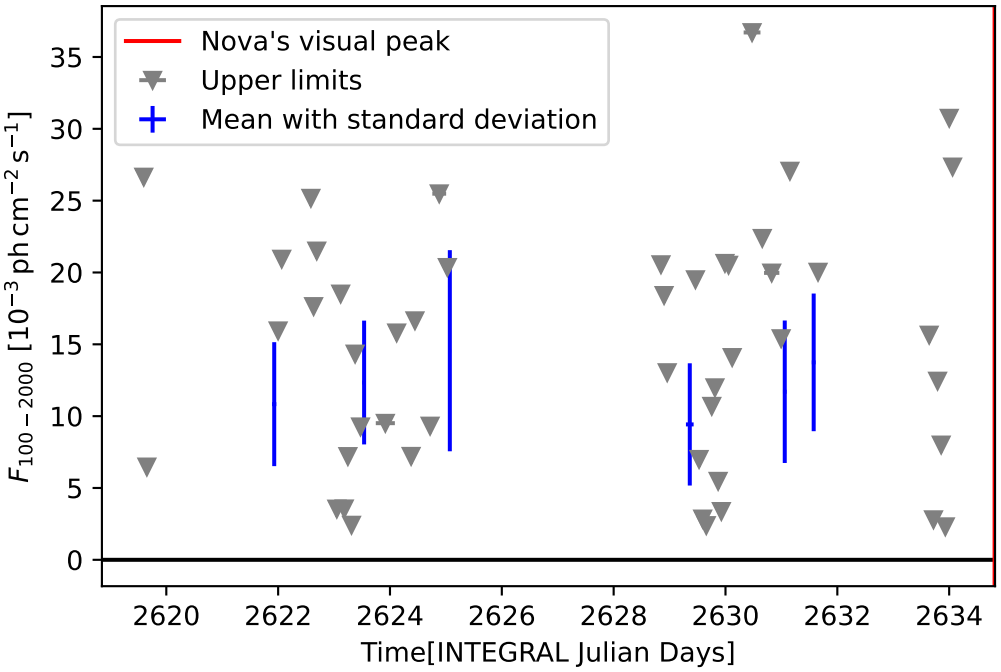

Figure A.4: Lightcurve of V2615 Oph

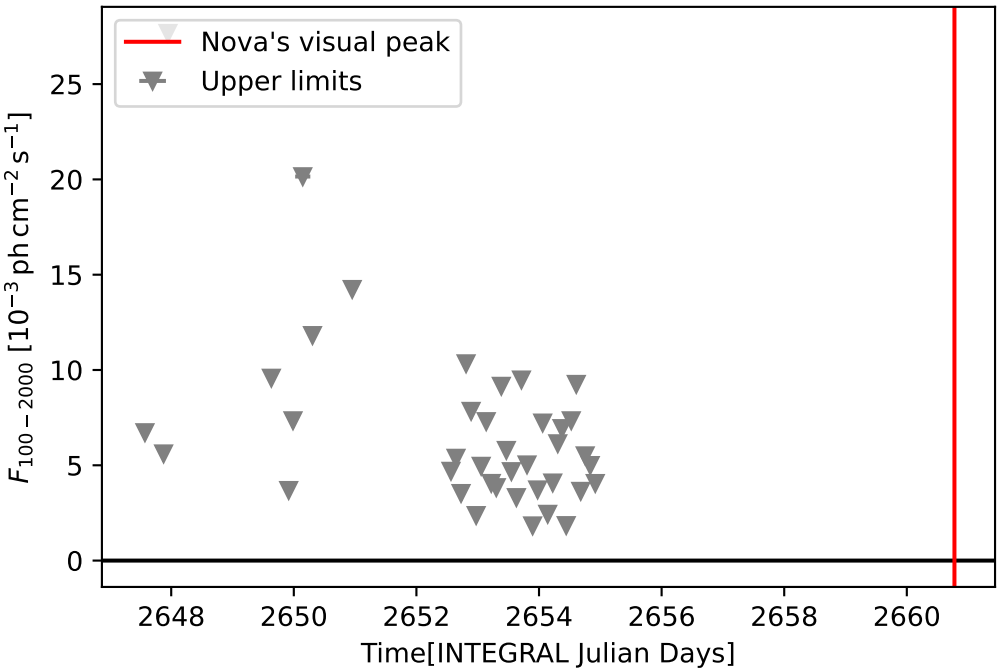

Figure A.5: Lightcurve of V5558 Sgr

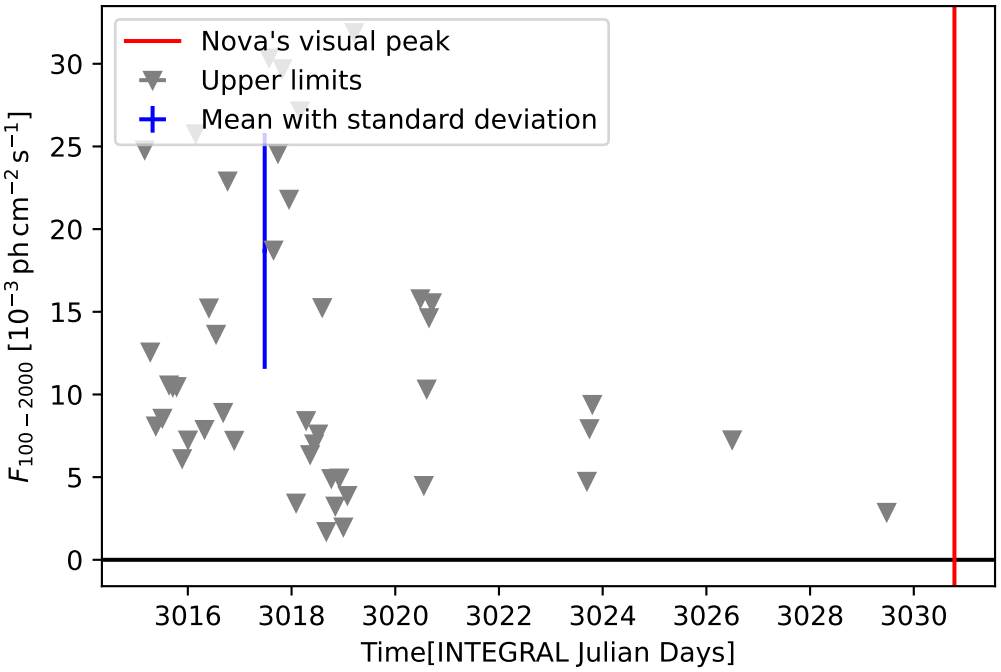

Figure A.6: Lightcurve of V5579 Sgr

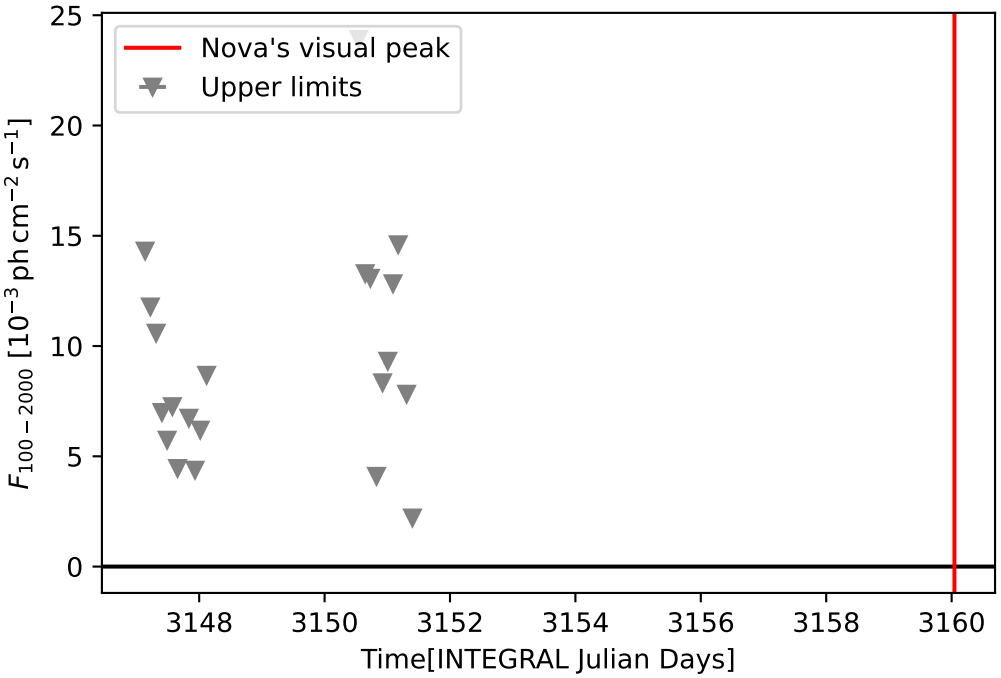

Figure A.7: Lightcurve of V1212 Cen

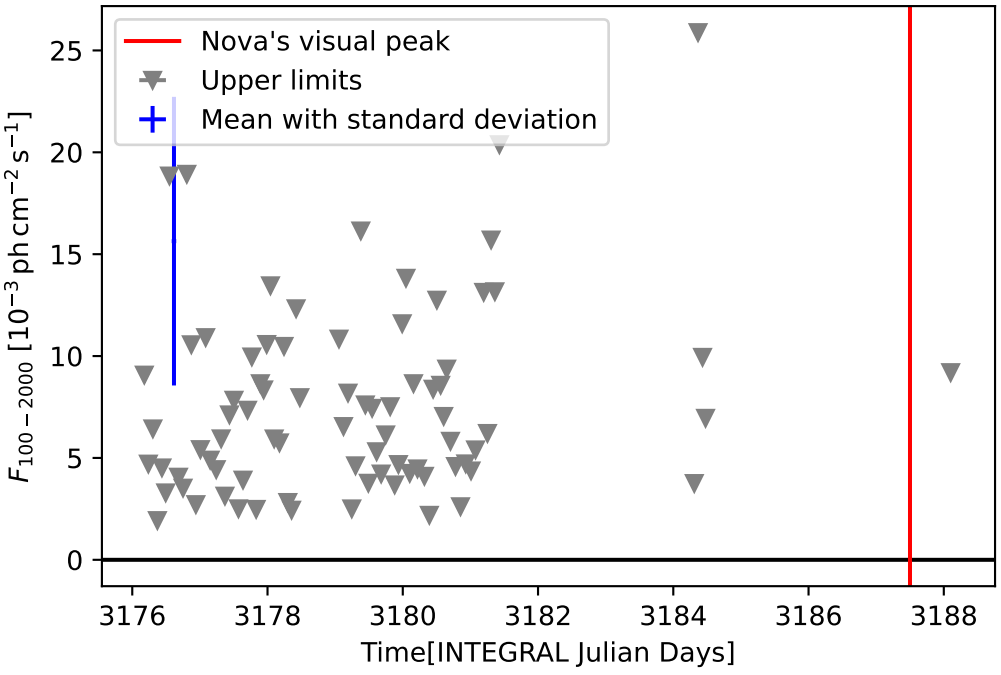

Figure A.8: Lightcurve of V1721 Aql

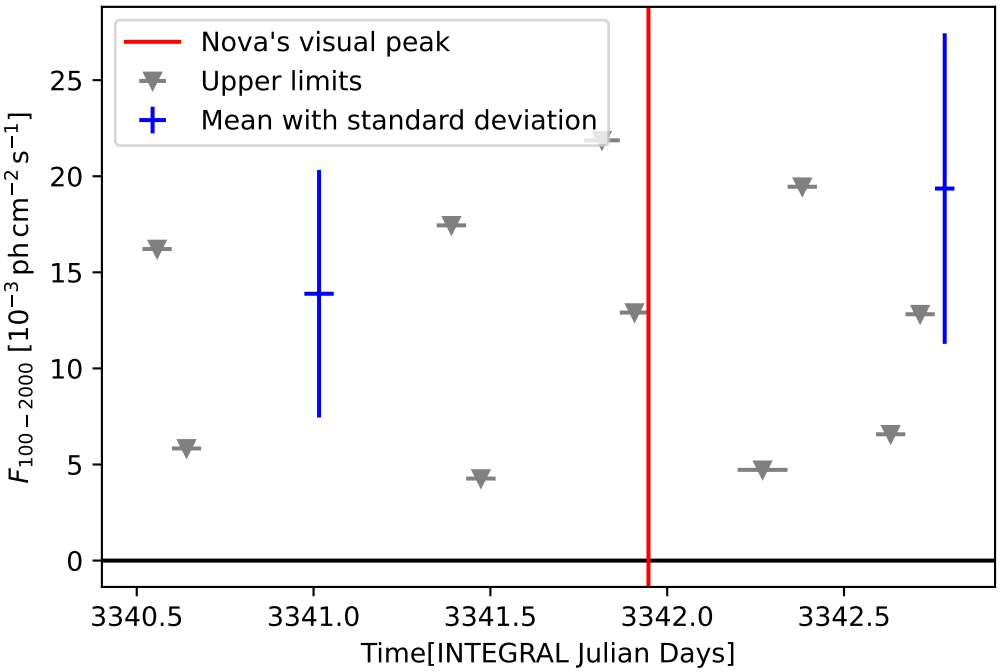

Figure A.9: Lightcurve of V5582 Sgr

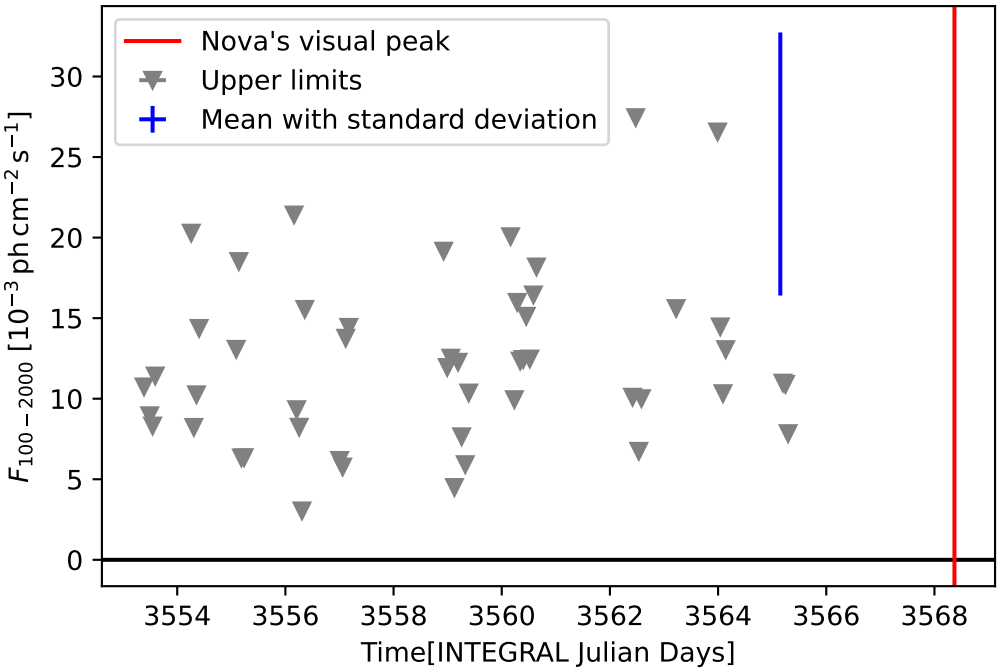

Figure A.10: Lightcurve of V496 Sct

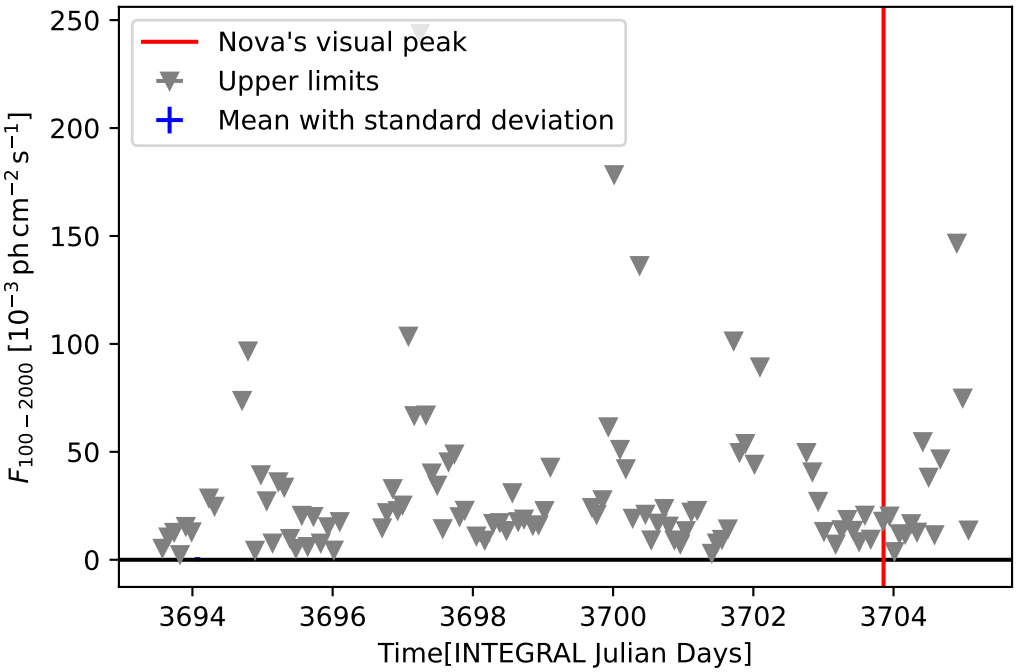

Figure A.11: Lightcurve of V1310 Sco

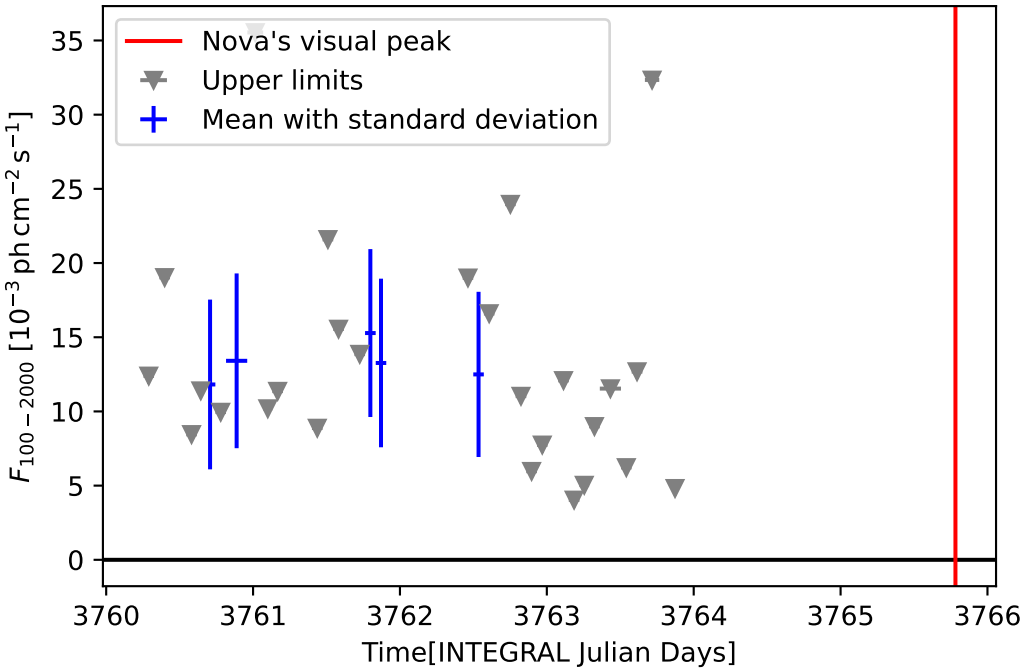

Figure A.12: Lightcurve of V5586 Sgr

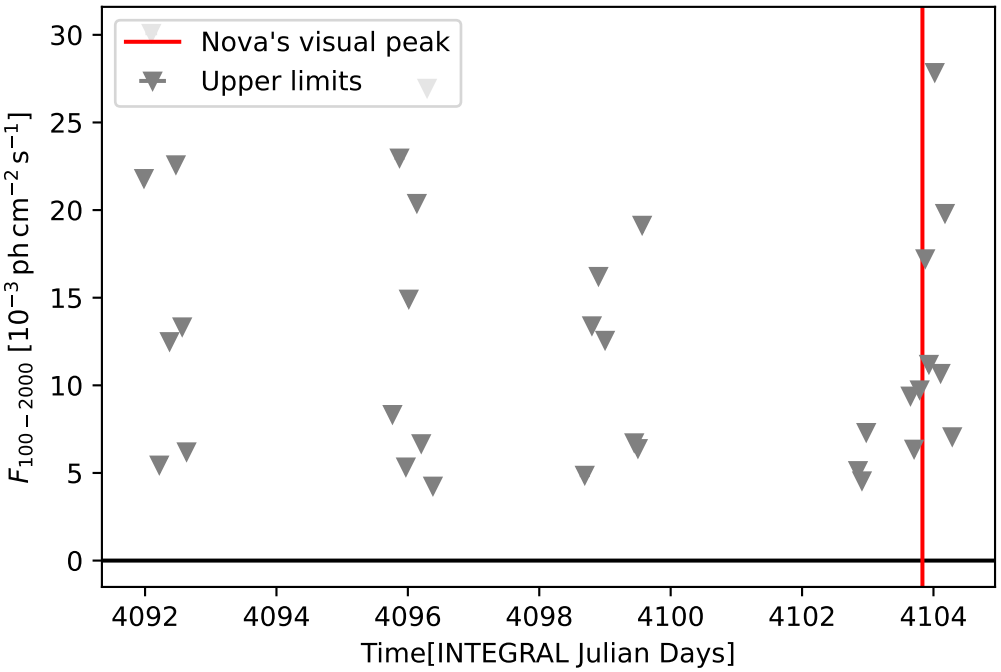

Figure A.13: Lightcurve of V5588 Sgr

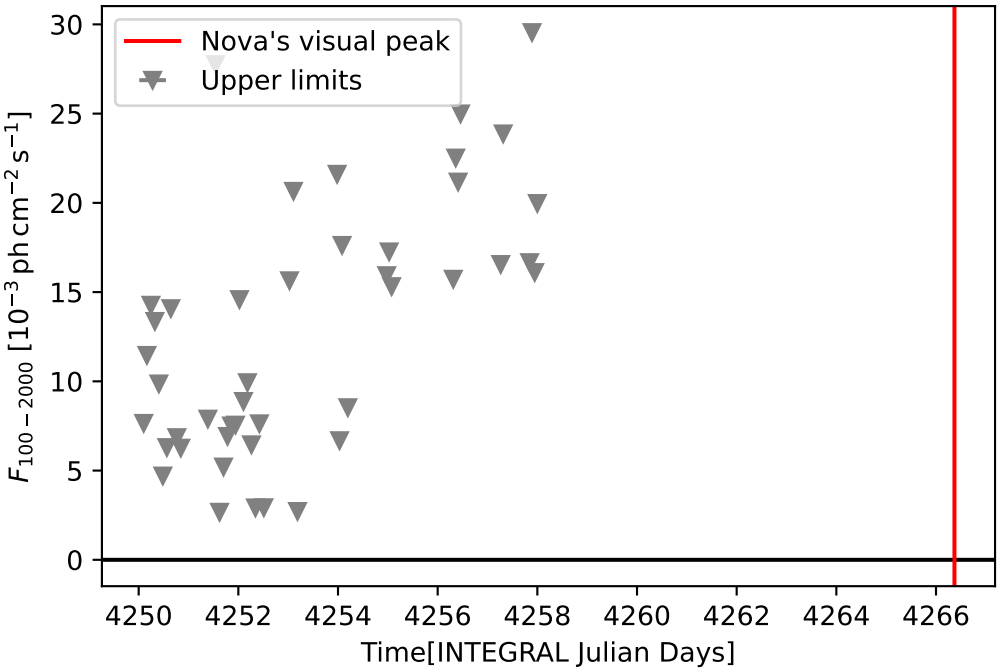

Figure A.14: Lightcurve of V1313 Sco

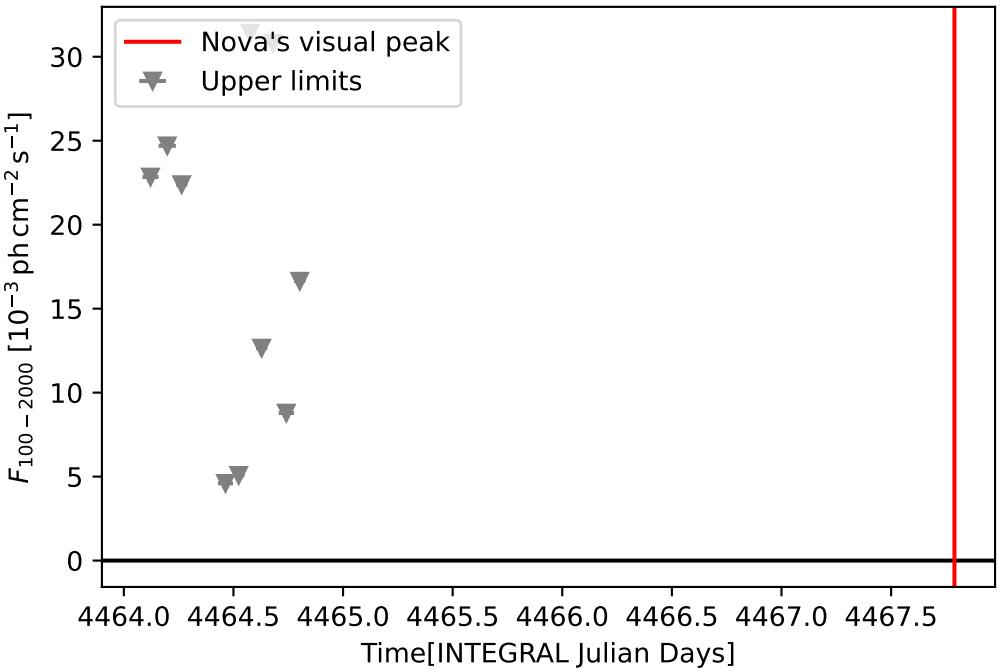

Figure A.15: Lightcurve of V2676 Oph

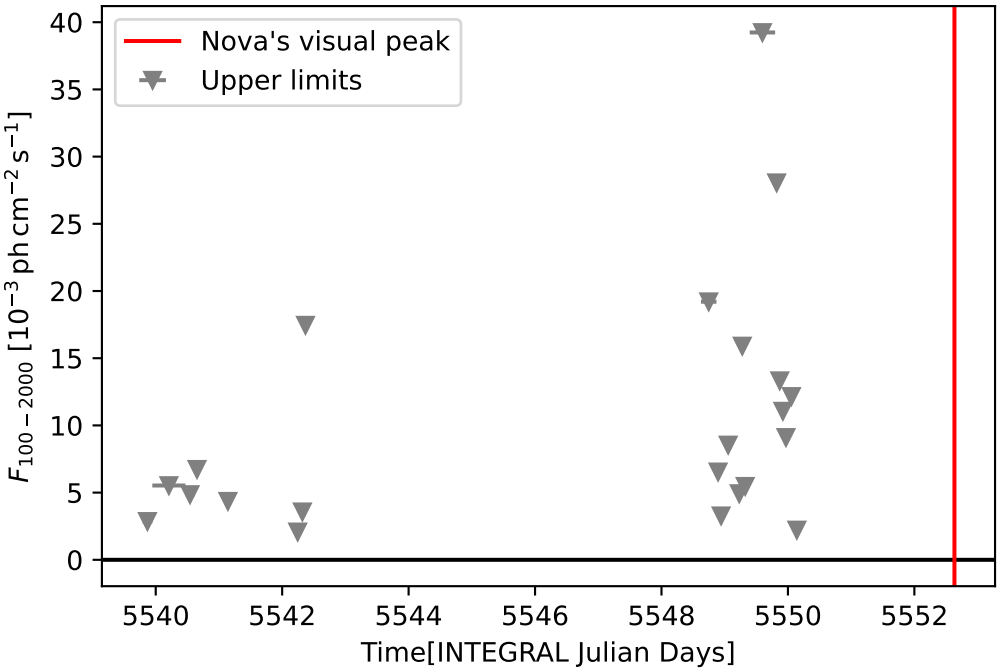

Figure A.16: Lightcurve of V5668 Sgr

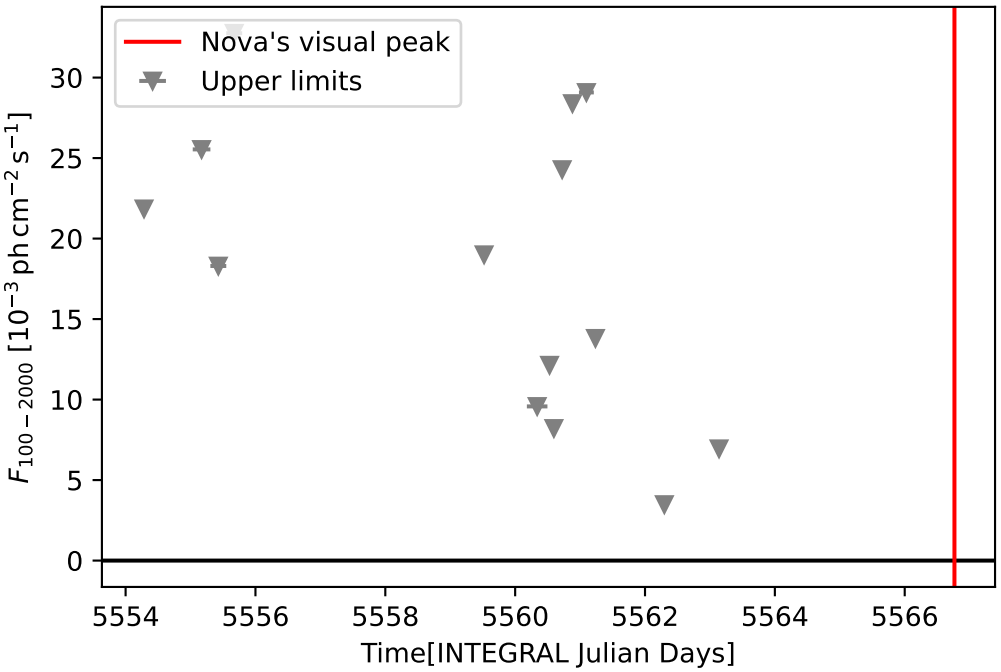

Figure A.17: Lightcurve of V2944 Oph

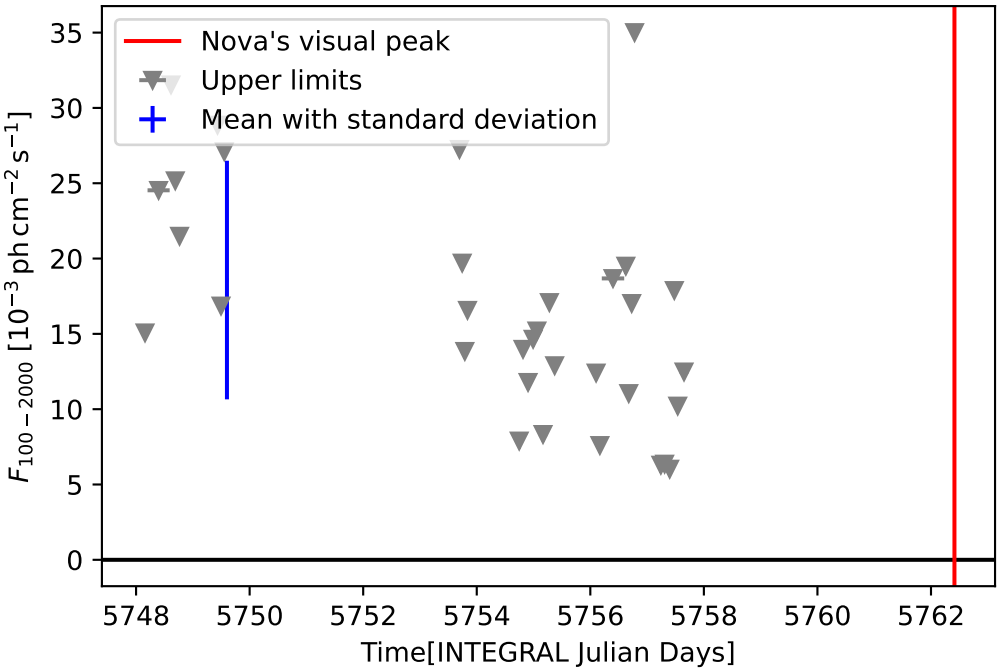

Figure A.18: Lightcurve of V2949 Oph

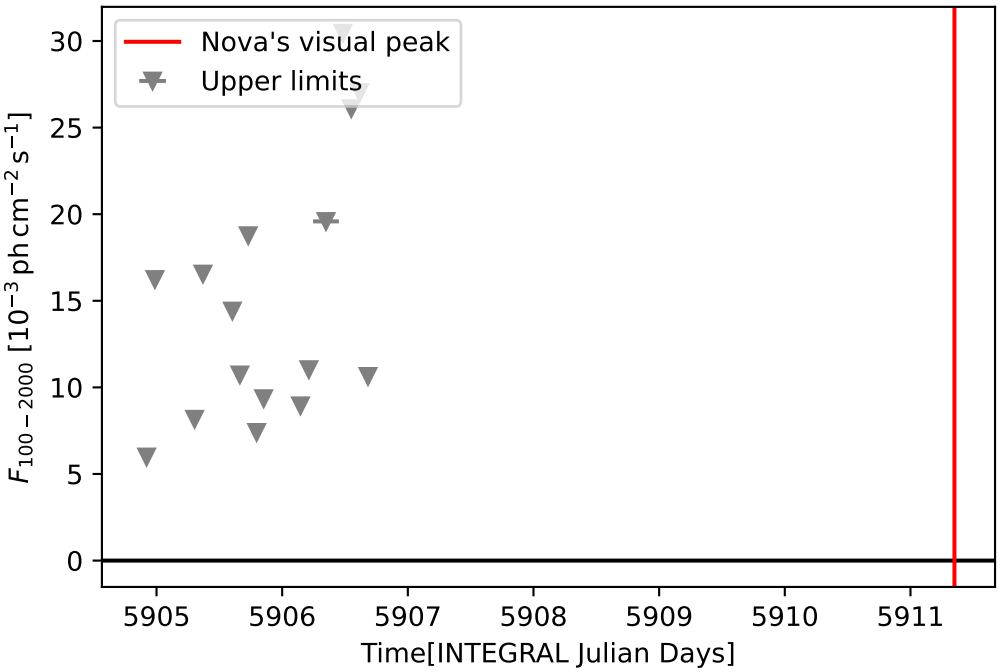

Figure A.19: Lightcurve of V555 Nor

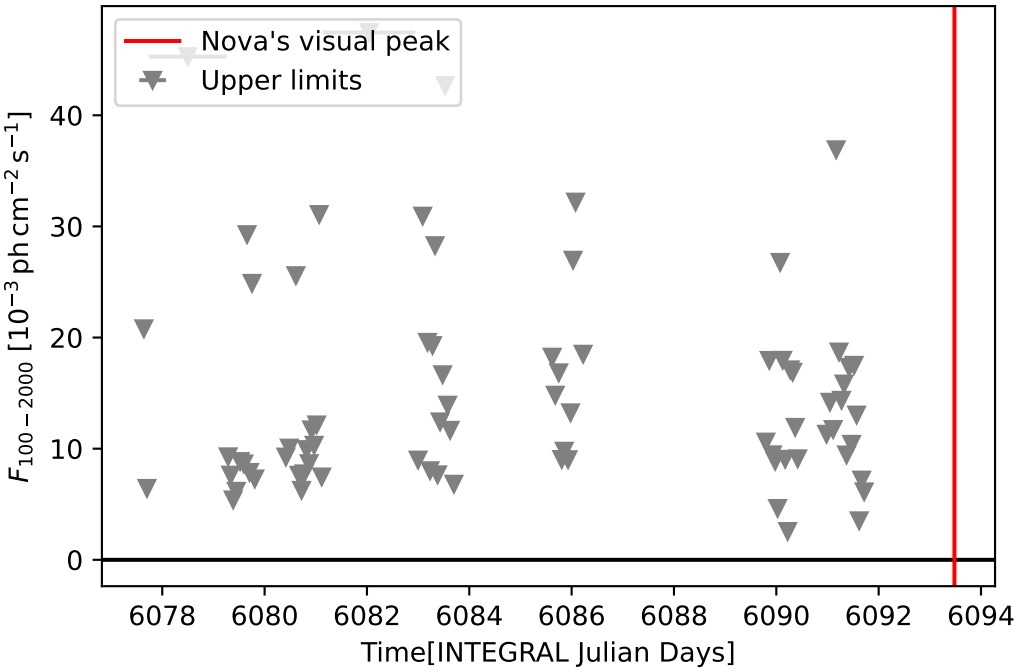

Figure A.20: Lightcurve of V1656 Sco

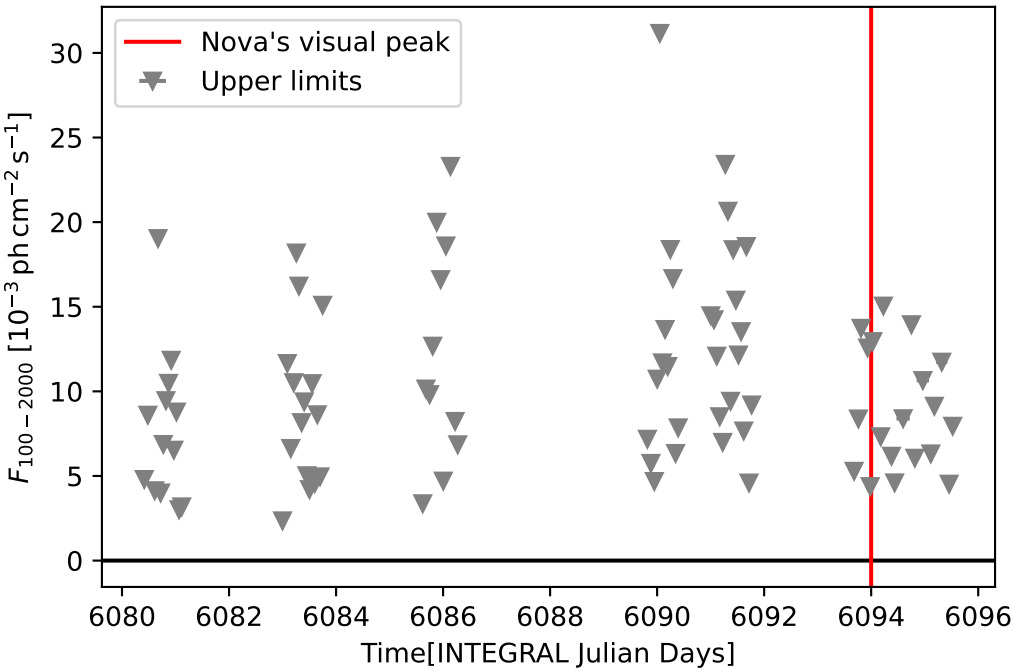

Figure A.21: Lightcurve of V1659 Sco

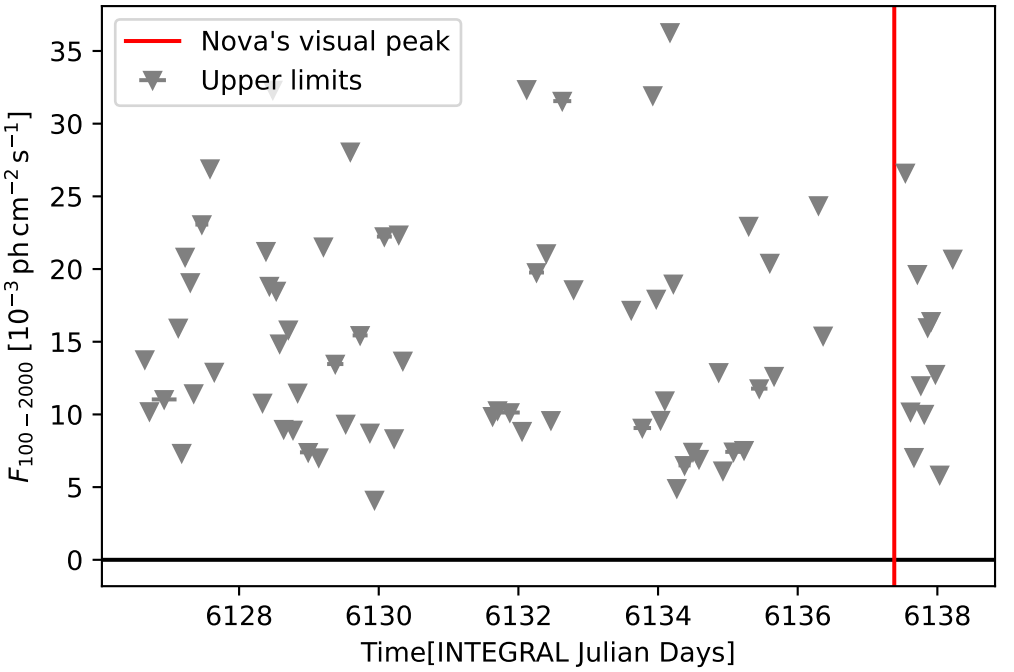

Figure A.22: Lightcurve of V5855 Sgr

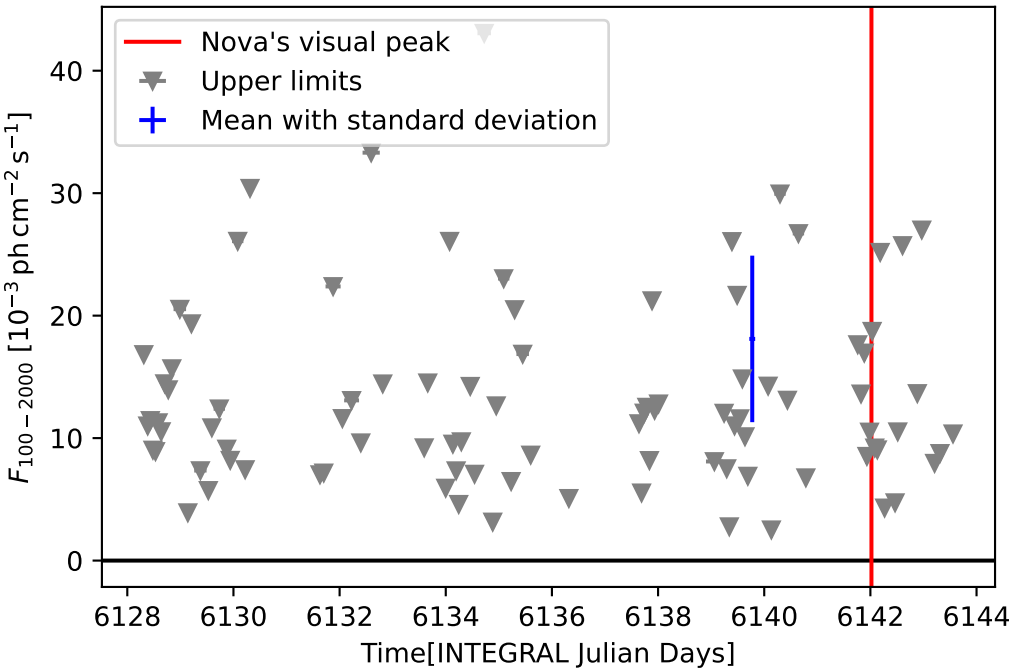

Figure A.23: Lightcurve of V5856 Sgr

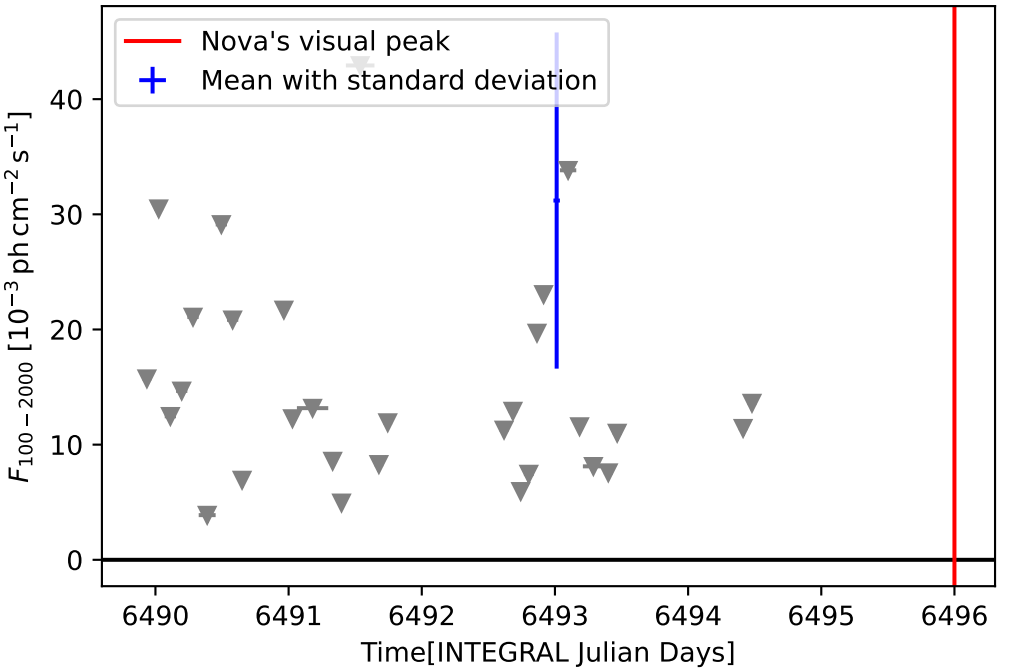

Figure A.24: Lightcurve of V1660 Sco

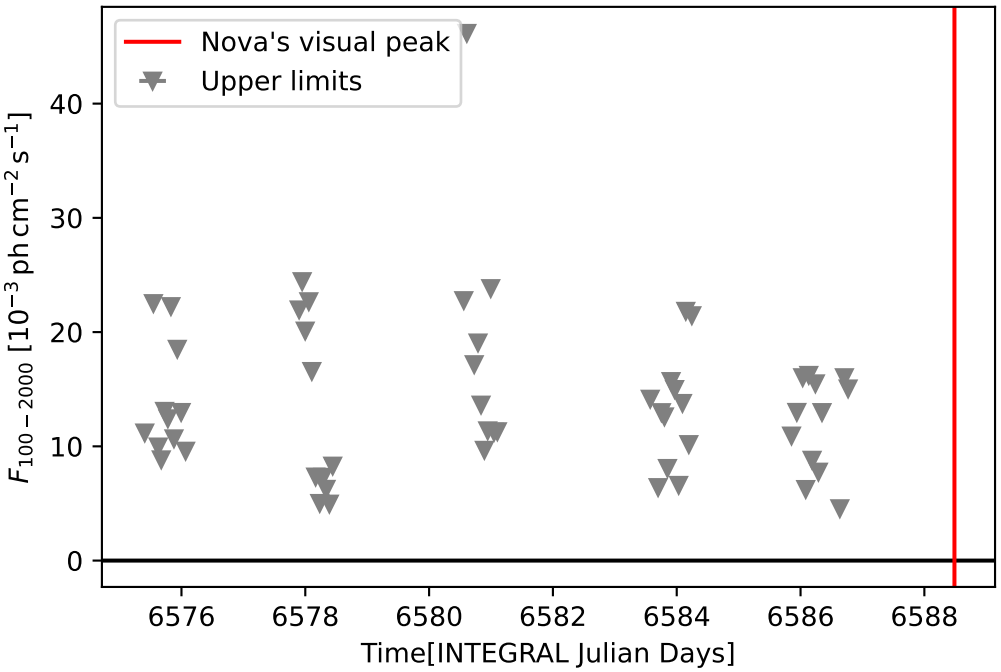

Figure A.25: Lightcurve of V357 Mus

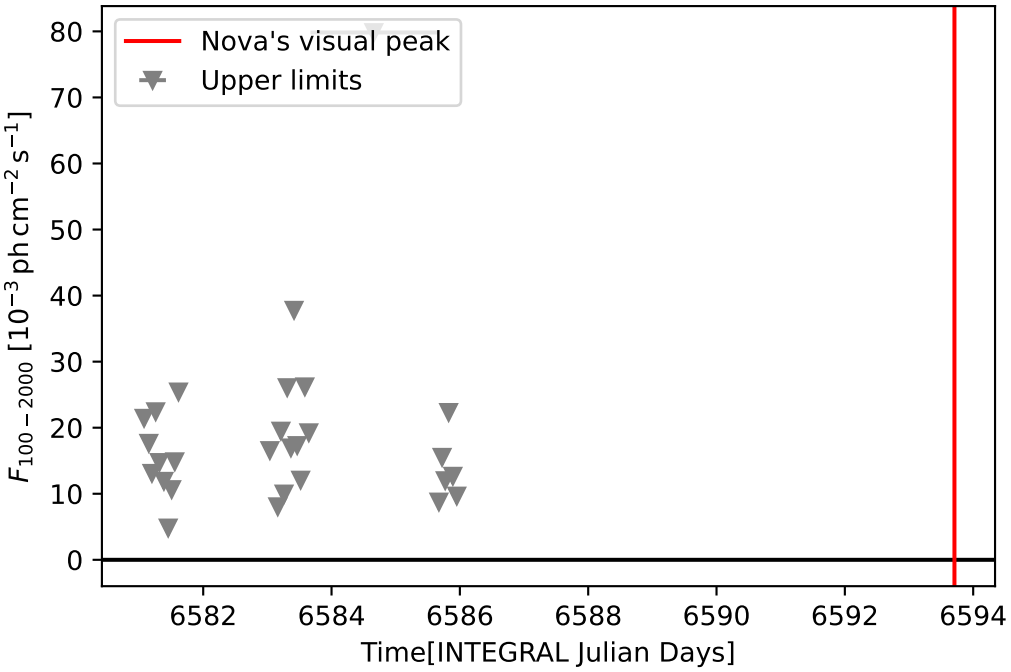

Figure A.26: Lightcurve of FM Cir

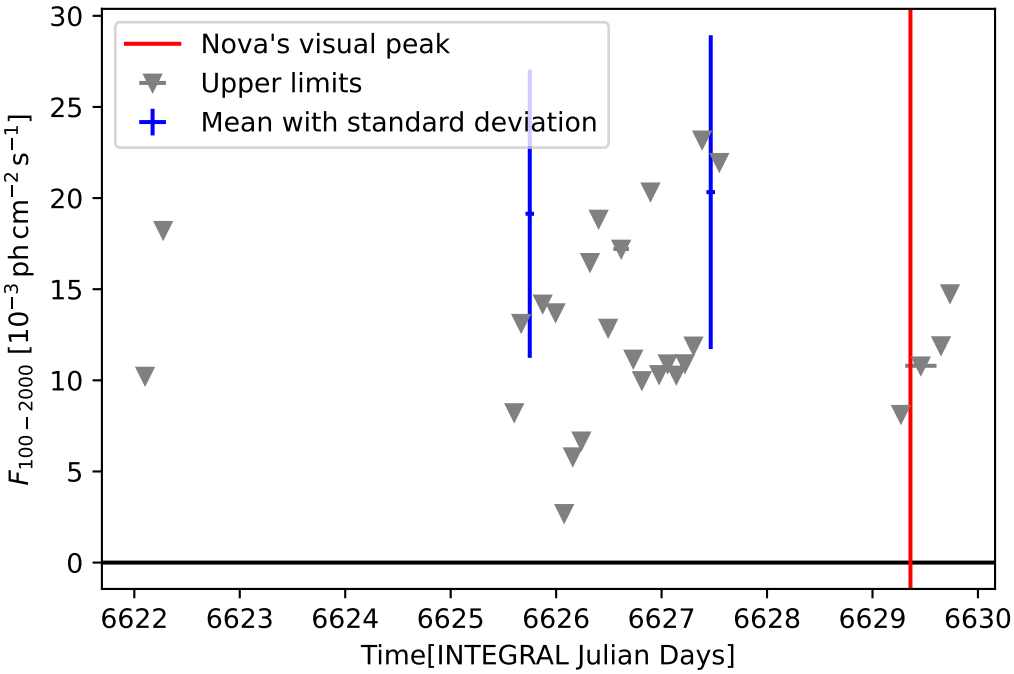

Figure A.27: Lightcurve of V1663 Sco

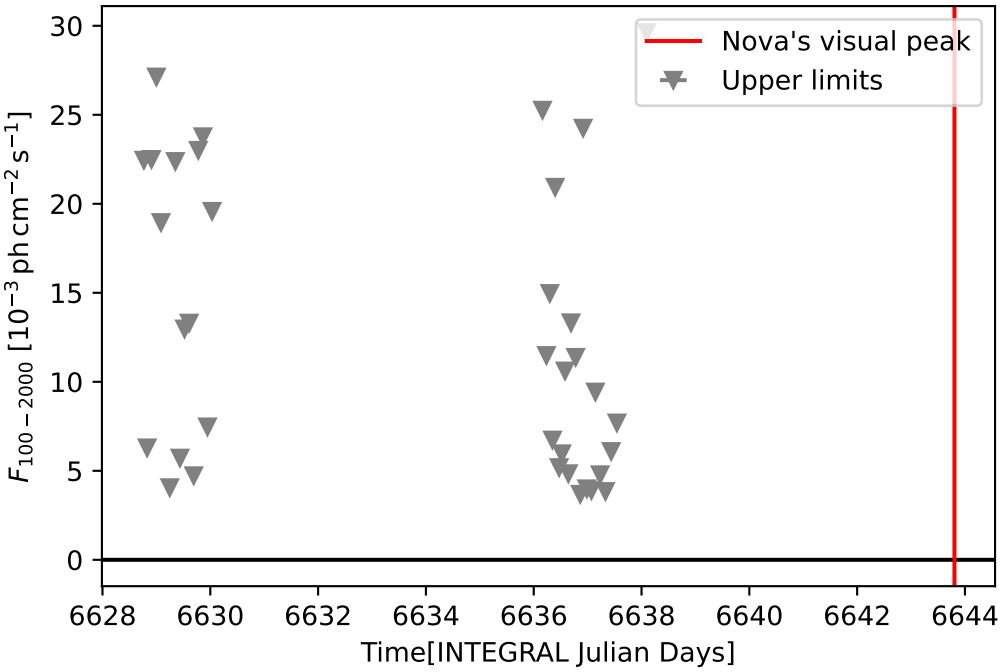

Figure A.28: Lightcurve of V3665 Oph

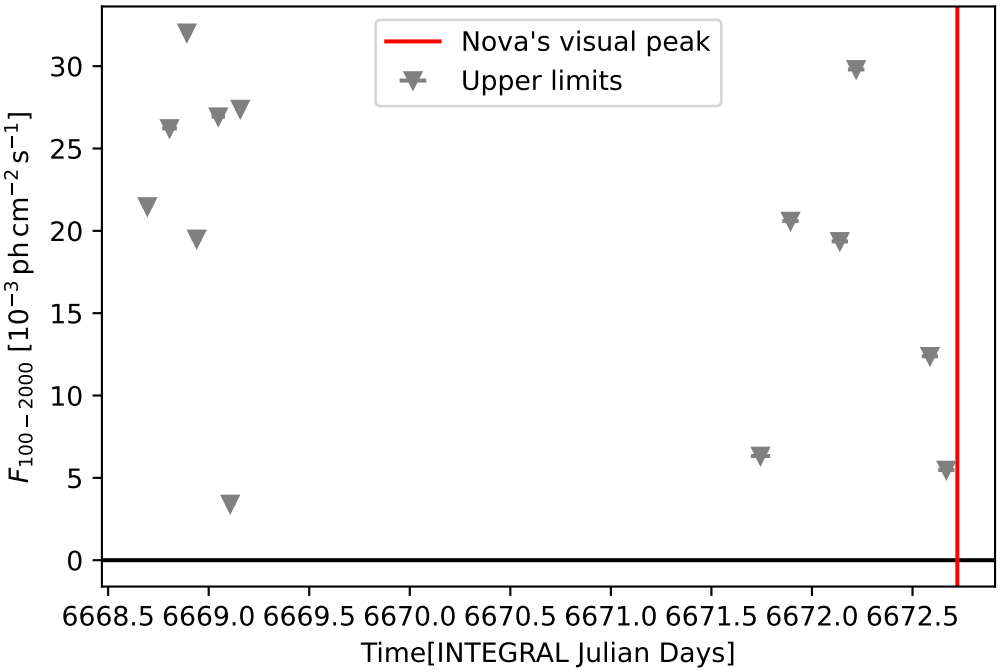

Figure A.29: Lightcurve of V5857 Sgr

Bibliography

[1] European Space Agency. *Integral overview*. 2022. URL: https://www.esa.int/Science_Exploration/Space_Science/Integral_overview.

[2] Rene Andrae, Tim Schulze-Hartung, and Peter Melchior. *Dos and don'ts of reduced chi-squared*. 2010. DOI: 10.48550/ARXIV.1012.3754. URL: https://arxiv.org/abs/1012.3754.

[3] Borb. *CNO cycle*. 2022. URL: https://supernova.eso.org/exhibition/images/0418_cno-1080/.

[4] Donald D. Clayton and Fred Hoyle. "Gamma-Ray Lines from Novae". In: 187 (Feb. 1974), p. L101. DOI: 10.1086/181406.

[5] Nick Connor. *What is Germanium Detector – Principle of Operation – Definition*. 2019. URL: https://www.radiation-dosimetry.org/what-is-germanium-detector-principle-of-operation-definition/.

[6] Roland Diehl et al. "INTEGRAL/SPI γ-ray line spectroscopy. Response and background characteristics". In: 611, A12 (Mar. 2018), A12. DOI: 10.1051/0004-6361/201731815. arXiv: 1710.10139 [astro-ph.IM].

[7] Roland Diehl et al. "SPI Measurements of Nucleosynthesis Gamma-Rays". In: (2013). DOI: 10.48550/ARXIV.1307.4190. URL: https://arxiv.org/abs/1307.4190.

[8] Rudolf Gross and Achim Marx. *Festkörperphysik*. Berlin, Germany: De Gruyter Studium, 2018.

[9] Izumi Hachisu and Mariko Kato. "A Universal Decline Law of Classical Novae. II. GK Persei 1901 and Novae in 2005". In: 662.1 (June 2007), pp. 552–563. DOI: 10.1086/517600. arXiv: astro-ph/0702563 [astro-ph].

[10] Frank A. Haight. *Handbook of the Poisson Distribution*. Cambridge, England: John Wiley Sons, Inc., 1967.

[11] M. Hernanz. *Gamma-ray emission from nova outbursts*. 2013. DOI: 10.48550/ARXIV.1305.0769. URL: https://arxiv.org/abs/1305.0769.

[12] Margarita Hernanz et al. "Gamma-Ray Emission from Novae Related to Positron Annihilation: Constraints on its Observability Posed by New Experimental Nuclear Data". In: 526.2 (Dec. 1999), pp. L97–L100. DOI: 10.1086/312372. arXiv: astro-ph/9910111 [astro-ph].

[13] Erik Kuulkers et al. "INTEGRAL reloaded: Spacecraft, instruments and ground system". In: 93, 101629 (Dec. 2021), p. 101629. DOI: 10.1016/j.newar.2021.101629.

[14] Shing-Chi Leung and Thomas Siegert. "Gamma-Ray Light Curves and Spectra of Classical Novae". In: *arXiv e-prints*, arXiv:2112.06893 (Dec. 2021), arXiv:2112.06893. arXiv: 2112.06893 [astro-ph.HE].

[15] Paul Murdin. *ENCYCLOPEDIA OF ASTRONOMY AND ASTROPHYSICS*. Hampshire, England: Nature Publishing Group, 2001.

[16] A. Neronov et al. "Online data analysis system of the INTEGRAL telescope". In: 651, A97 (July 2021), A97. DOI: 10.1051/0004-6361/202037850. arXiv: 2002.12895 [astro-ph.IM].

[17] Aykut Özdönmez et al. "The distances of the Galactic novae". In: 461.2 (Sept. 2016), pp. 1177–1201. DOI: 10.1093/mnras/stw1362. arXiv: 1606.01907 [astro-ph.SR].

[18] Dubath P. et al. *SPI Analysis User Manual*. 2005. URL: http://isdc.unige.ch/integral/download/osa/doc/10.2/osa_um_spi.pdf.

[19] Richard J. Rossi. *Mathematical statistics: an introduction to likelihood based inference*. Cambridge, England: John Wiley Sons, Inc., 2018.

[20] A. W. Shafter. "The Galactic Nova Rate Revisited". In: 834.2, 196 (Jan. 2017), p. 196. DOI: 10.3847/1538-4357/834/2/196. arXiv: 1606.02358 [astro-ph.SR].

[21] Michael M. Shara et al. "The Masses and Accretion Rates of White Dwarfs in Classical and Recurrent Novae". In: *The Astrophysical Journal* 860.2 (June 2018), p. 110. DOI: 10.3847/1538-4357/aabfbd. URL: https://doi.org/10.3847%2F1538-4357%2Faabfbd.

[22] Thomas Siegert, Deirdre Horan, and Gottfried Kanbach. "Telescope Concepts in Gamma-Ray Astronomy". In: *arXiv e-prints*, arXiv:2207.02248 (July 2022), arXiv:2207.02248. arXiv: 2207.02248 [astro-ph.HE].

[23] Thomas Siegert et al. "Background modelling for γ-ray spectroscopy with INTEGRAL/SPI". In: 626, A73 (June 2019), A73. DOI: 10.1051/0004-6361/201834920. arXiv: 1903.01096 [astro-ph.HE].

[24] Thomas Siegert et al. "Nucleosynthesis constraints through γ-ray line measurements from classical novae. Hierarchical model for the ejecta of ^{22}Na and ^{7}Be". In: 650, A187 (June 2021), A187. DOI: 10.1051/0004-6361/202140300.

[25] Adie Alegoric Stewart. *Electromagnetic Spectrum*. 2022. URL: https://wiki.travellerrpg.com/Electromagnetic_Spectrum.

[26] B. J. Teegarden and S. J. Sturner. "INTEGRAL Observations of Gamma-Ray Bursts". In: AAS/High Energy Astrophysics Division 4, 17.01 (Apr. 1999), p. 17.01.

[27] G. Vedrenne et al. "SPI: The spectrometer aboard INTEGRAL". In: 411 (Nov. 2003), pp. L63–L70. DOI: 10.1051/0004-6361:20031482.

[28] Frederick M. Walter et al. "The Stony Brook/SMARTS Atlas of (mostly) Southern Novae". In: *Publications of the Astronomical Society of the Pacific* 124.920 (Oct. 2012), pp. 1057–1072. DOI: 10.1086/668404. URL: https://doi.org/10.1086%2F668404.

[29] C. Winkler et al. "The INTEGRAL mission". In: 411 (Nov. 2003), pp. L1–L6. DOI: 10.1051/0004-6361:20031288.